

FILE COPY

AD-A223 971

**THE SCOUR OF COHESIVE SOILS  
BY AN INCLINED SUBMERGED WATER JET**

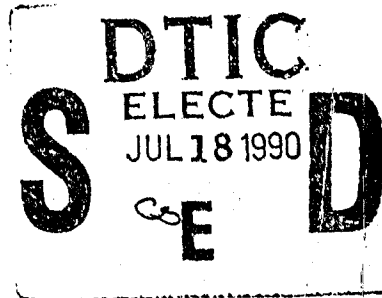
A Thesis

by

JOSEPH DELBERT HEDGES

Submitted to the Office of Graduate Studies of  
Texas A&M University  
in partial fulfillment of the requirements for the degree of  
**MASTER OF SCIENCE**

May 1990



Major Subject: Ocean Engineering

90 07 17 039

**THE SCOUR OF COHESIVE SOILS  
BY AN INCLINED SUBMERGED WATER JET**

A Thesis  
by  
**JOSEPH DELBERT HEDGES**



Accession For	
NTIS GRA&I	<input checked="" type="checkbox"/>
DTIC TAB	<input type="checkbox"/>
Unannounced	<input type="checkbox"/>
Justification	<i>form 502</i>
by _____	
Distribution/	
Availability Codes	
Dist	Avail and/or Special
<i>A-1</i>	

Submitted to the Office of Graduate Studies of  
Texas A&M University  
in partial fulfillment of the requirements for the degree of  
**MASTER OF SCIENCE**

May 1990

Major Subject: Ocean Engineering

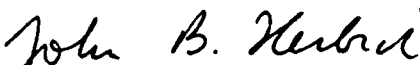
**THE SCOUR OF COHESIVE SOILS  
BY AN INCLINED SUBMERGED WATER JET**


**A Thesis**

**by**

**JOSEPH DELBERT HEDGES**

**Approved as to style and content by:**

  
\_\_\_\_\_  
**John B. Herbich**  
**(Chair of Committee)**

  
\_\_\_\_\_  
**Aubrey L. Anderson**  
**(Member)**

  
\_\_\_\_\_  
**Wayne Alan Dunlap**  
**(Member)**

\_\_\_\_\_  
**J. T. P. Yao**  
**(Head of Department)**

**May 1990**

**ABSTRACT****The Scour of Cohesive Soils**

by an Inclined Submerged Water Jet. (May 1990)

Joseph Delbert Hedges,

B.S., California State University, Chico

Chair of Advisory Committee: Dr. John B. Herbich

A physical model test consisting of a vertically inclined submerged turbulent jet impinging upon a horizontal brick-like clay sample was conducted. Using dimensional analysis the controlling parameters were identified. The data was collected and analyzed to determine the functional relationships between time duration of scour impingement, shear strength of clay, distance of separation between sample and jet, and angle of inclination of jet. It was shown that a linear relationship existed between the scour volume and time of impingement. Furthermore, a relationship existed between the shear strength of the clay and the scour rate and volume. However, the primary governing parameter of scour rate and volume was the tractive shear stress resulting from the impinging jet. The tractive shear stress was varied by changing the angle of inclination and distance of separation of the jet. *Thesis 1990*

### ACKNOWLEDGMENTS

This thesis is dedicated to my family.

To my wife, : Thank you for standing by me. Without your advice, support and love, I would still be working on Chapter I. I love you.

To my children: Thank you for the "little helping hands".

To my parents : Thank you for giving me so many opportunities throughout the years. Your sacrifices have not gone unnoticed.

I am deeply indebted to my Committee for their support and advice. A special note of thanks to Dr. J. B. Herbich and Dr. W. A. Dunlap whose words of wisdom lead me out of many a quandary. Also, a special note of thanks to Celeste Simmons, DJ Blockhus, Mike Barrett, and Craig Jones for their support and hard work. Last and by no means least, thanks to the U.S. Navy for the privilege of attending Texas A&M University.

# TABLE OF CONTENTS

	PAGE
ABSTRACT .....	iii
ACKNOWLEDGMENTS .....	iv
TABLE OF CONTENTS .....	v
LIST OF TABLES .....	vii
LIST OF FIGURES .....	viii
CHAPTER	
I INTRODUCTION .....	1
GENERAL .....	1
HYPOTHESIS .....	1
EXPERIMENT .....	2
SPECIFIC OBJECTIVES .....	3
II LITERATURE REVIEW .....	4
CLAYS .....	4
Properties .....	4
Shear Strength and Plasticity .....	7
SCOUR .....	10
FLOW THROUGH AN ORIFICE .....	15
FLUID RADIAL JET .....	17
III DIMENSIONAL ANALYSIS .....	23
IV EXPERIMENTAL APPARATUS AND EQUIPMENT .....	26
VANE SHEAR DEVICE .....	26
CLAY .....	26
MODEL TEST .....	28
WATER SOURCE .....	37
V EXPERIMENTAL PROCEDURE .....	40
SAMPLE PREPARATION .....	40
SOUR ANALYSIS .....	41
JET THRUST ANALYSIS .....	45
JET VELOCITY ANALYSIS .....	45

CHAPTER	PAGE
VI ANALYSIS OF RESULTS .....	46
JET VELOCITY .....	46
JET THRUST .....	49
SCOUR VOLUME .....	51
SCOUR RATE .....	66
SCOUR GEOMETRY .....	74
VII CONCLUSIONS AND RECOMMENDATIONS .....	81
REFERENCES .....	85
APPENDICES .....	88
APPENDIX I - NOTATION .....	89
APPENDIX II - SCOUR ANALYSIS RESULTS.....	91
APPENDIX III- THRUST ANALYSIS RESULTS .....	102
APPENDIX IV - VELOCITY ANALYSIS RESULTS.....	107
VITA .....	113

## LIST OF TABLES

TABLE		PAGE
1	Test Program .....	43
2	Initial Velocity of Jet .....	47



## LIST OF FIGURES

FIGURE		PAGE
1	Typical Results of Drained Shear Test .....	9
2	Typical Results of Undrained Shear Test .....	9
3	Vertical Jet Apparatus .....	13
4	Flow Through an Orifice .....	16
5	Submerged Radial Jet Mixing Diagram .....	20
6	Normal Probability Curve of Radial Jet Mixing	20
7	Laboratory Vane Shear Device .....	27
8	In Situ Vane Shear Device .....	27
9	Atterberg Limit Results .....	29
10	Vane Shear Strength vs Water Content Percentage .....	29
11	Cinva Ram .....	30
12	Orifice .....	31
13	Orifice Sketch .....	31
14	Scour Apparatus .....	33
15	Scour Apparatus Sketch .....	33
16	Pressure Transducer Box Sketch .....	34
17	Thrust Apparatus .....	35
18	Thrust Apparatus Sketch .....	35
19	Velocity Apparatus .....	36
20	Velocity Apparatus Sketch .....	36
21	Main and Control Valves .....	39
22	Clay Sample .....	42

FIGURE	PAGE
23 Normal Distribution of Jet. $y_J = 1.0$ ft .....	48
24 Dimensionless Normal Center Line Pressure Resulting from Jet Thrust vs Distance of Separation .....	50
25 Dimensionless Scour Volume vs Time. $\beta = 90^\circ$ and $z/d = 13.33$ .....	52
26 Dimensionless Scour Volume vs Time. $\beta = 90^\circ$ and $z/d = 16.00$ .....	52
27 Dimensionless Scour Volume vs Time. $\beta = 90^\circ$ and $z/d = 18.66$ .....	53
28 Dimensionless Scour Volume vs Time. $\beta = 90^\circ$ and $z/d = 21.33$ .....	53
29 Dimensionless Scour Volume vs Time. $\beta = 75^\circ$ and $z/d = 13.33$ .....	54
30 Dimensionless Scour Volume vs Time. I of II. $\beta = 75^\circ$ and $z/d = 16.00$ .....	54
31 Dimensionless Scour Volume vs Time. II of II. $\beta = 75^\circ$ and $z/d = 16.00$ .....	55
32 Dimensionless Scour Volume vs Time. $\beta = 75^\circ$ and $z/d = 18.66$ .....	55
33 Dimensionless Scour Volume vs Time. I of IV. $\beta = 60^\circ$ and $z/d = 13.33$ .....	55
34 Dimensionless Scour Volume vs Time. II of IV. $\beta = 60^\circ$ and $z/d = 13.33$ .....	56
35 Dimensionless Scour Volume vs Time. III of IV. $\beta = 60^\circ$ and $z/d = 13.33$ .....	57
36 Dimensionless Scour Volume vs Time. IV of IV. $\beta = 60^\circ$ and $z/d = 13.33$ .....	57
37 Dimensionless Scour Volume vs Time. I of II. $\beta = 60^\circ$ and $z/d = 16.00$ .....	58
38 Dimensionless Scour Volume vs Time. II of II. $\beta = 60^\circ$ and $z/d = 16.00$ .....	58
39 Dimensionless Scour Volume vs Time. $\beta = 60^\circ$ and $z/d = 18.66$ .....	59

FIGURE	PAGE
40 Dimensionless Scour Volume vs Time. $\beta = 45^\circ$ and $z/d = 13.33$ .....	60
41 Dimensionless Scour Volume vs Time. $\beta = 45^\circ$ and $z/d = 16.00$ .....	60
42 Dimensionless Scour Volume vs Time. $\beta = 45^\circ$ and $z/d = 18.66$ .....	61
43 Dimensionless Scour Volume vs Angle of Inclination. $z/d = 13.33$ .....	64
44 Dimensionless Scour Volume vs Angle of Inclination. $z/d = 16.00$ .....	64
45 Dimensionless Scour Volume vs Angle of Inclination. $z/d = 18.66$ .....	65
46 Dimensionless Scour Volume vs Normal Surface Pressure. $z/d = 13.33$ .....	67
47 Dimensionless Scour Volume vs Normal Surface Pressure. $z/d = 16.00$ .....	67
48 Dimensionless Scour Volume vs Normal Surface Pressure. $z/d = 18.66$ .....	68
49 Dimensionless Rate of Scour vs Shear Strength. $\beta = 90^\circ$ .....	70
50 Dimensionless Rate of Scour vs Shear Strength. $\beta = 75^\circ$ .....	70
51 Dimensionless Rate of Scour vs Shear Strength. $\beta = 60^\circ$ .....	71
52 Dimensionless Rate of Scour vs Shear Strength. $\beta = 45^\circ$ .....	71
53 Dimensionless Rate of Scour vs Distance .....	72
54 Dimensionless Rate of Scour vs Normal Surface Pressure .....	72
55 Scour. Sample No. B-III. $z/d = 16.00$ , $\beta = 90^\circ$ , $V_o \cdot t/d = 7.20 \times 10^5$ .....	75
56 Scour. Sample No. B-III. $z/d = 16.00$ , $\beta = 90^\circ$ , $V_o \cdot t/d = 1.44 \times 10^6$ .....	76

## FIGURE

## PAGE

57	Scour. Sample No. B-III. $z/d = 16.00$ , $\beta = 90^\circ$ , $V_o \cdot t/d = 2.16 \times 10^6$ .....	77
58	Scour. Sample No. B-I. $z/d = 16.00$ , $\beta = 60^\circ$ , $V_o \cdot t/d = 7.20 \times 10^5$ .....	78
59	Scour. Sample No. B-I. $z/d = 16.00$ , $\beta = 60^\circ$ , $V_o \cdot t/d = 1.44 \times 10^6$ .....	79
60	Scour. Sample No. B-I. $z/d = 16.00$ , $\beta = 60^\circ$ , $V_o \cdot t/d = 2.16 \times 10^6$ .....	80

## CHAPTER I

### INTRODUCTION

#### GENERAL

The study of submerged cohesive incline scour resulting from a turbulent water jet has many applications in Coastal Engineering. One such application is the prediction and prevention of localized scour of narrow ship channels due to ship thruster usage. According to Pinson (23), surface ships commonly use thrusters to gain autonomy from tug services. Thrusters provide maneuverability in restricted narrow channels. These thrusters produce a concentrated and powerful jet-like force profile, as described by Stuntz and Taylor (28), that impinges upon the bank of the narrow channel. The result is localized scour which eventually leads to bank erosion and slope instability. The bank erosion causes sediment to be transported into the channel reducing its navigable depth, and causes lateral retreat as a result of slope instability. Also, the study of cohesive incline scour can be applied to improving the efficiency of jet assisted draghead dredging as described by Herbich (12), and developing new technology for offshore trenching as

---

The citations on the following pages follow the style of the *Journal of Waterway, Port, Coastal and Ocean Engineering*, ASCE.

described by Tausig (29).

## **HYPOTHESIS**

This study was centered around the hypothesis that the rate and volume of scour of inclined cohesive soils, due to a submerged, turbulent, fluid jet is a function of the following parameters:

- 1) Time duration of turbulent scour impingement,
- 2) Shear strength of clay,
- 3) Angle of inclination of slope, and
- 4) Characteristics of the submerged water jet causing turbulent scour.

## **EXPERIMENT**

A survey of available literature reveals that published material concerning the scour of cohesive inclines is very limited. Thus, the purpose of this study was to investigate this scour phenomenon and its controlling parameters. To achieve this, a physical model study was conducted. Terra Cotta clay was molded into brick-like samples and impinged upon by a vertically inclined, submerged water jet. The jet was inclined instead of the sample's surface. This allowed the sample's surface to remain in the horizontal plane minimizing the effects of gravity. Thus, slope stability was negated as a controlling parameter.

The following parameters were varied for given time durations to investigate their relationships to scour:

- 1) Shear Strength of the clay was varied by increasing or decreasing the clay's water content,
- 2) Thrust of Jet on clay sample was varied by changing the distance from jet's discharge opening to sample's surface and angle of inclination of jet.

#### **SPECIFIC OBJECTIVES**

The specific objectives of this study were:

- 1) To examine the velocity and thrust profiles of the water jet; and
- 2) To determine the relationships between scour rate and volume with respect to:
  - (a) time duration of scour impingement,
  - (b) shear strength of clay,
  - (c) distance of jet from sample, and
  - (d) angle of inclination of jet.

## CHAPTER II

### LITERATURE REVIEW

#### CLAYS

##### Properties

Cernica (7), and Holtz and Kovacs (14) describe a cohesive soil as the result of the atomic bonding of individual clay tetrahedral and octahedral crystalline complexes to form sheets. The crystalline complexes form sheets of repeating atomic structure by sharing common ions in their lattice structure. The sheets are attracted together or repulsed by Van der Waals and Coulombic forces, as described by Allen and Keefer (4). They stack together to form plate-like particles that are finer than 2 microns. The plate-like particles have a net negative charge, a large surface area per unit weight (specific surface), and vary greatly in size depending upon the clay.

The crystalline complexes are comprised of hydrous aluminosilicates and other metallic ions whose origin is the chemical weathering of certain rock-forming minerals, primarily feldspathic rock. The tetrahedral crystalline complex is a combination of a single silica cation surrounded by four oxygen anions at each corner. The oxygen anions at the bases of each tetrahedron are in one



plane with the unjoined anions all pointed in the same direction. Two tetrahedron crystalline complexes share one base anion bonding the tetrahedron crystallines into sheets. The octahedral crystalline complex is a combination of an aluminum, magnesium, iron or other metallic ion surrounded by six oxygen or hydroxyl anions. The rows of oxygen or hydroxyl anions are in two planes.

The type and quantity of cations along with anions in the crystalline lattice structure dictate the type of clay. The particular way in which these sheets stack together (i.e., octahedral to octahedral, or tetrahedral to octahedral) further dictate the type of clay.

Clay minerals are strongly influenced by the presence of water because of the crystalline electrostatic field and large lattice structure surface area, and water's polar molecular bonding characteristics. Water is said to be "adsorbed" by the clay because a molecular bond forms between the water molecule and clay mineral. Water is a dipole which infers that it is electrically neutral with separate positive and negative centers of charge. The water molecule is electrostatically attracted to the negatively charged anions in crystalline lattice structure forming a water film that can be several water molecules thick. Generally, as the water content increases, the adsorbed water that surrounds the clay mineral grows in thickness. This oriented water zone is termed the "diffuse double layer". Thus, the larger the specific

surface, the greater the influence of the increased water content.

Also, free positively-charged cations known as "exchangeable cations" are attracted to the negatively charged crystalline surface. These cations can be easily exchanged and are predominantly monovalent sodium and potassium. The divalent calcium and magnesium cations with iron and aluminum occur on less common occasions. Dunlap (9) states, "In general terms, the higher valence cations can displace those of lower valence although this process can be reversed if the higher valence cations are overwhelmed by a large number of lower valence cations." These cations cause the diffuse double layer to vary its thickness depending upon the cation. Sowers and Sowers (27) describe the molecular bonding mechanisms of the water dipole and exchangeable cations as follows:

1. The dipole (electrostatic attraction).
2. Hydrogen bonding (the sharing of hydrogen atoms with the clay, and
3. Hydration of the cations that are attracted to the clay surface to compensate for isomorphous substitution.

The thickness of the diffuse double layer causes the sheets making up a particle to be physically separated by a given distance. The thinner the diffuse layer, the greater the sheet attraction and molecular bonding strength causing reduced potential movement between

sheets. As the water content increases the plasticity increases and shear strength decreases.

### Shear Strength and Plasticity

The shear strength and plasticity of a clay soil is a direct function of its electrochemical environment and physical characteristics as discussed above. Being able to quantitatively measure and describe these properties allows the behavior of clays with respect to scour to be predicted.

As described by Sowers and Sowers (27), and Dunlap (9), a saturated clay is relatively compressible allowing an applied load to be initially supported by the pore water pressure between particles and not the soil structure. Furthermore, the low permeability of clays does not allow the generated pore pressures to be dissipated rapidly.

The shear strength of a soil is determined by applying a shear stress,  $\tau$ , to a sample causing failure along a plane during a triaxial or direct shear test, Cernica (7) and Taylor (30). During a "drained" test the normal stress,  $\sigma_{11}$ , is applied and the clay is allowed to consolidate. The consolidation reduces the sample's void ratio and water content prior to shear failure. Thus, the shear strength of a sample will increase proportionally because of increased particle to particle friction as shown in Fig. 1. The slope of a straight line

representing shear stress with respect to normal stress is termed the "angle of friction",  $\phi_D$ . Typical values for the angle of friction are between  $15^\circ$  and  $30^\circ$ . The smaller the angle the lower the clay's plastic index.

This line does not pass through the origin and has an initial value,  $C_D$ , for preconsolidated clays. After preconsolidation, particles do not return to their original spacing and higher void ratio. However, for this to occur the excess water molecules released from the double diffuse layer due to increased normal stress must be allowed to drain from the sample to reduce pore pressure. The line will pass through the origin for normally consolidated clays.

In the "undrained" test the water is not allowed to drain from the sample during consolidation or shear. The initial shear strength,  $C_u$ , will remain constant with respect to increasing normal stress as shown in Fig. 2, and the angle of friction,  $\phi_u$ , will be equal to zero. Since no consolidation occurs, the water content of the clay will not vary causing the shear strength to remain constant. This method is most commonly used to measure the shear strength of clays, and can be easily determined with a vane shear apparatus.

The plasticity range of a clay can be used as a measure of cohesiveness and can be defined by its Atterberg Limits as follows:

- 1) The "liquid limit", LL, is the water content in

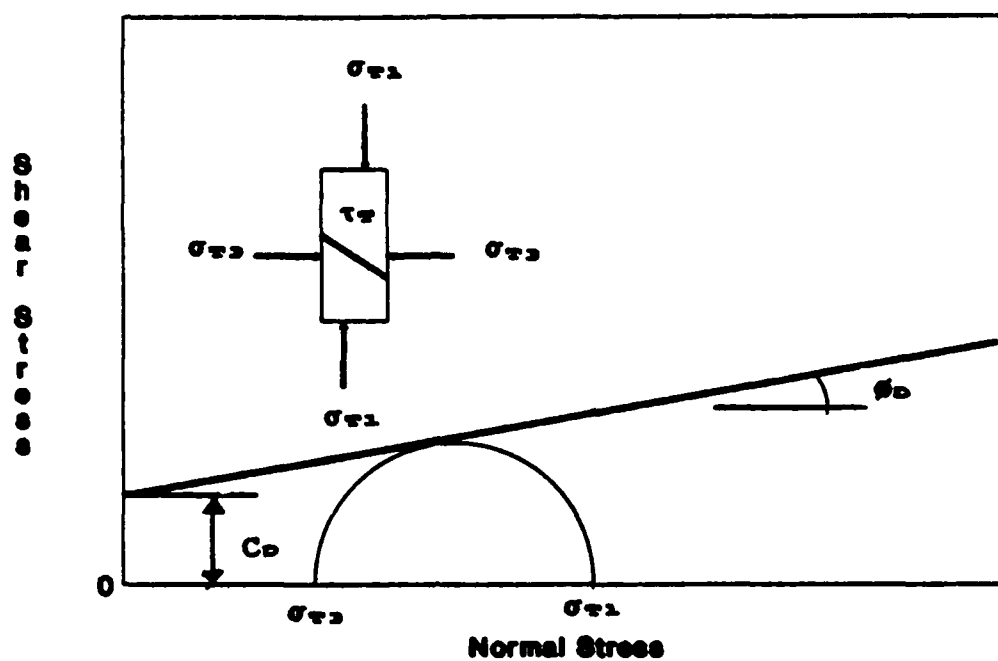


FIG. 1.-Typical Results of Drained Shear Test ( Ref. 7, 9, 27, and 31).

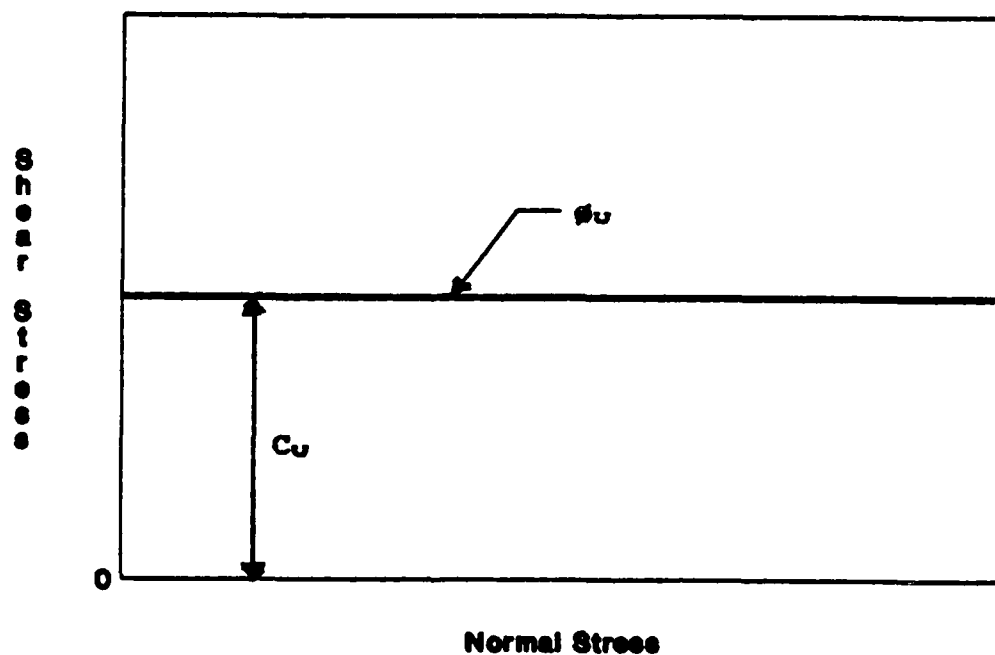


FIG. 2.-Typical Results of Undrained Shear Test (Ref. 6, 9, 27 and 31).

percentage by weight of dry sediment at which the sediment exhibits a small shearing strength as determined by the Casagrande liquid limit device.

- 2) The "plastic limit", PL, is the water content in percentage by weight of dry sediment at which the sediment begins to crumble when rolled into thin cylinders.
- 3) The "plastic index",  $I_p$ , is the difference between the liquid and plastic limits. The greater the plastic index the stronger the inter-sheet bonding with respect to the growth of the double diffuse layer. Thus, a high plastic index indicates high adsorption and repulsion, large interparticle spacing, and correspondingly less interparticle attraction.

## SCOUR

There has been limited study into the scour of cohesive soils on an incline as the result of jet thrust, but the majority of work concludes that the severity of scour will be a function of the clay's physico-chemical characteristics and environment as described by Middleton (20). Vanoni (31) reports that increasing clay particle size, plasticity index, and shear stress will decrease scour severity. According to Laursen (17), "Scour can be defined as the enlargement of a flow section by the

removal of material composing the boundary through the action of the fluid of motion. Implicit in this definition is the fact that the moving fluid exerts forces on the particles comprising the boundary." Thus, the scour of a submerged and inclined cohesive soil initiated by jet thrust is an extremely complex problem due to the difficulty in defining the boundary conditions and the intrinsic properties of the cohesive soil.

Abt, Ruff, and Shaikh (2) observed that the mechanisms of erosion varied in three clays tested which resulted in different rates of scour. Their experiment consisted of placing flat samples on the bottom of a tilting flume with a constant water velocity running over the samples to cause erosion. The Na-montmorillonite eroded particle by particle at the slowest rate. Next was the kaolinite which eroded by colloidal dispersion, detachment and removal of large soil aggregates with sizes up to 5 mm. The fastest was Ca-montmorillonite which eroded in large masses due to slaking. Furthermore, their results showed a linear relationship between the magnitude of erosion and sample shear stress. Na-montmorillonite and Ca-montmorillonite showed a linear relationship between the magnitude of erosion and time, but kaolinite did not. Bhasin, Lovell, and Toebe (5) verified that both relationships exist in their study of the erosion of sand-clay mixtures subjected to a submerged vertical water jet.

Smerdon and Beasley (26) observed that the critical tractive force increased as the percentage of clay in the sample increased and also as the plastic index of the samples increased. They tested soils ranging from silty loam to clay in a tilting flume.

Dunn (10) using a submerged vertical water jet placed above a sample, Fig. 3, was able to formulate the critical tractive (boundary) shear with respect to the soil's shear strength and plastic index as follows

$$\tau_c = 0.001(C_u + 180)\tan(30 + 1.73 \cdot I_p) \dots\dots\dots (1)$$

where

$C_u$  = undrained soil shear strength (lbs/ft<sup>2</sup>),

$I_p$  = plastic index, and

$\tau_c$  = critical tractive shear (lbs/ft<sup>2</sup>).

Eq. 1 is valid for soils with a plastic index between 5 and 16. However, Partheniades (22) working with San Francisco marine muds concluded that the critical tractive force is not a function of consolidation or shear stress. He concluded the critical tractive shear depends upon the bond strength of clay flocs.

Masch and Moore (19) used the same apparatus as Dunn (10) and determined the depth of erosion was proportional to the logarithm of duration of the experiment for natural and composite cohesive sediments as follows

$$K_s = f\{ (p \cdot V_o \cdot d)/\mu, (C_u \cdot p \cdot d^2)/\mu^2 \} \dots\dots\dots (2)$$

$$s/h = K_s \cdot \log(t \cdot \mu / p \cdot d^2) \dots\dots\dots (3)$$

where



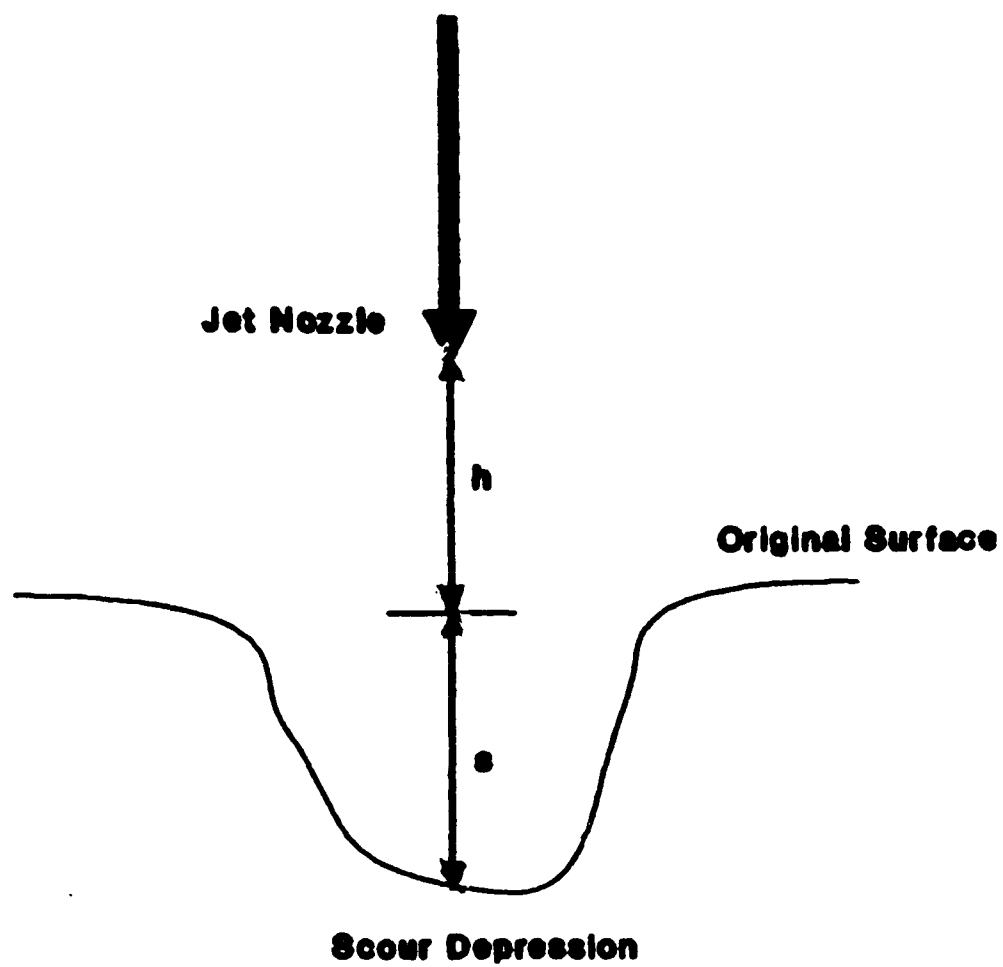


FIG. 3.-Vertical Jet Apparatus (Ref. 10 and 19).

$C_u$  = Undrained soil shear strength (lb/ft<sup>2</sup>),

$d$  = diameter of jet nozzle (ft),

$K_s$  = proportionality constant,

$s$  = depth of scour depression (ft),

$t$  = time duration of scour (ft),

$V_o$  = jet velocity at nozzle (ft/sec),

$\rho$  = mass density of water (slug/ft<sup>3</sup>), and

$\mu$  = dynamic viscosity of water (lb·sec/ft<sup>2</sup>).

Abdel-Rahmann (1), using a flume apparatus similar to Abt, Ruff, and Shaikh (2) also determined that the depth of scour with respect to duration of scour is a logarithmic relationship.

Herbich (13) stated that studies using an apparatus similar to Dunn (10), predicted the erosion rate equations as follows

$$Q_m = 3.43 - 0.03 \cdot C_u \dots\dots\dots (4)$$

where

$C_u$  = undrained soil shear strength (kg/m<sup>2</sup>), and

$Q_m$  = volumetric erosion rate (m<sup>3</sup>/sec).

Also utilizing the jet velocity and distance the erosion rate can be predicted as follows

$$Q_m = C_1 \cdot (V_o/h - C_2) \dots\dots\dots (5)$$

where

$C_1$  = constant

$C_2$  = constant

$h$  = vertical distance of separation between jet and sample (ft),

$Q_e$  = volumetric erosion rate ( $\text{ft}^3/\text{sec}$ ), and

$V_o$  = jet velocity at nozzle, ( $\text{ft}/\text{sec}$ ).

$C_1$  is equal to 0.07 and  $C_2$  is equal to 38.6 for a jet of diameter 3/16 inch.

Dunn (10) also noted that the initial scour occurred a short distance away from the center line of the jet. The location of the initial scour was unaffected by changes in either the nozzle head or the elevation of the nozzle above the sample. However, Herbich (13) stated that once scour was initiated its geometry could be predicted by the ratio of elevation of jet above sample to jet diameter as follows

$$h/d < 10 \quad \text{local scour pit} \quad \dots\dots\dots (6)$$

$$h/d > 10 \quad \text{wider and planer scour} \quad \dots\dots\dots (7)$$

#### FLOW THROUGH AN ORIFICE

Denn (8) and Olsen (21) define an orifice as a plate with a small, sharp-edged hole placed in a flowing stream as shown by Fig. 4. Assuming uniform velocity and incompressibility, the continuity equation is as follows

$$A_1 \cdot V_1 = A_o \cdot V_o = Q \quad \dots\dots\dots (8)$$

where

$A_o$  = cross sectional area at orifice ( $\text{ft}^2$ ),

$A_1$  = cross sectional area at point 1 ( $\text{ft}^2$ ),

$Q$  = volumetric flow rate ( $\text{ft}^3/\text{sec}$ ),

$V_o$  = velocity at orifice ( $\text{ft}/\text{sec}$ ), and

$V_1$  = velocity at point 1 ( $\text{ft}/\text{sec}$ ).

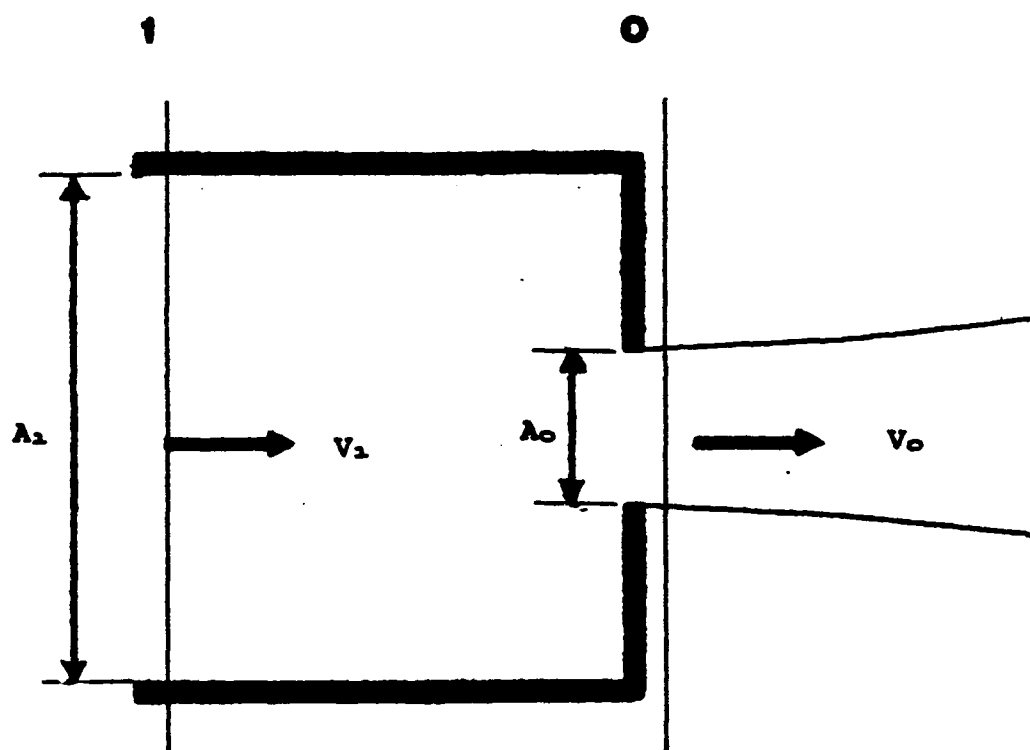


FIG. 4.-Flow Through an Orifice (Ref. 8 and 21).

The ideal Bernoulli equation neglecting constricting head loss and energy correction factor terms can be written as follows

$$V_1^2/2 = V_o^2/2 + (P_o - P_1)/\rho \quad \dots\dots\dots (9)$$

where

$P_o$  = pressure at orifice (lb/ft<sup>2</sup>),

$P_1$  = pressure at point 1 (lb/ft<sup>2</sup>), and

$\rho$  = mass density of water (slug/ft<sup>3</sup>).

Combining Eq. 8 with Eq. 9 results in the following

$$Q = A_1(2 \cdot g \cdot h_L)^{1/2} / [1 - (A_1/A_o)^2]^{1/2} \quad \dots\dots\dots (10)$$

where

$g$  = gravity constant, and

$h_L$  = pressure head lost (ft).

Eq. 10 can be simplified further, and constricting and energy correction terms can be accounted for with the introduction of a flow coefficient as follows

$$Q = K \cdot A_o \cdot (2 \cdot g \cdot h_L)^{1/2} \quad \dots\dots\dots (11)$$

where

$K$  = flow coefficient.

The flow coefficient is approximately equal to 0.62 and is a function of the following parameters

$$K = F \{ A_o/A_1, V_1 \cdot d/\mu \} \quad \dots\dots\dots (12)$$

where

$\mu$  = dynamic viscosity of water (lb-sec/ft<sup>2</sup>).

#### FLUID RADIAL JET

Poreh, Tsuei, and Cermak (24) state that the

submerged flow field formed by a steady impinging turbulent jet on a inclined boundary plane, as shown by Fig. 5, can be divided into the following four zones: zone of flow establishment, zone of established flow, impinging zone, and wall jet.

Immediately downstream from the nozzle exists the zone of flow establishment. This zone rapidly diminishes away from the nozzle due to shear stress according to Rajaratnam (25). The velocity distribution at the nozzle is assumed to be relatively constant causing a pronounced velocity discontinuity between the jet and surrounding fluid. The discontinuity generates eddies causing radial mixing at the boundary. At the boundary the jet is gradually decelerated and the surrounding fluid is accelerated resulting in a radial slowing of the constitutionalist core. The center line velocity will remain the initial nozzle velocity. However, the rate of flow entrainment and width of jet will increase with respect to distance away from the nozzle. The center line length of this zone is approximately six discharge opening diameters.

The next region is the zone of established flow. In this zone the central part of the jet has become turbulent therefore the diffusion process continues essentially unchanged thereafter. Further entrainment of the surrounding fluid by the expanding eddy region is now balanced by a continuous reduction in the velocity of the

entire central region. This will cause the slope of the jet's nominal boundary to increase upon reaching this zone to approximately 1 to 5. Albertson, et al. (3), used volume flux, momentum flux, and energy flux to develop a set of equations for this zone. The radial velocity distribution of this zone can be simulated by the normal distribution as shown by Fig. 6 as follows

$$V/V_M = \exp(-z_J^2/2 \cdot \sigma_s^2) \quad \text{.....} \quad (13)$$

where

$V$  = velocity parallel to the jet axis at a radial distance from the center line (ft/sec),

$V_M$  = velocity parallel to the jet along the center line in the zone of established flow (ft/sec),

$z_J$  = radial distance from center line (ft), and

$\sigma_s$  = standard deviation of velocity profile (ft).

The standard deviation,  $\sigma_s$ , can be represented by the radial distance from the center line to a point at which  $V_s$  occurs. The equation for  $V_s$  is as follows

$$V_s = 0.605 \cdot V_M \quad \text{.....} \quad (14)$$

where

$V_s$  = velocity parallel to the jet axis along the center line at one standard deviation (ft/sec).

The velocity, flow entrainment, and kinetic energy can be predicted for the zone of established flow as follows

$$V_M/V_0 = 6.2/(y_J/d) \quad \text{.....} \quad (15)$$

$$Q_M/Q = 0.32 \cdot (y_J/d) \quad \text{.....} \quad (16)$$

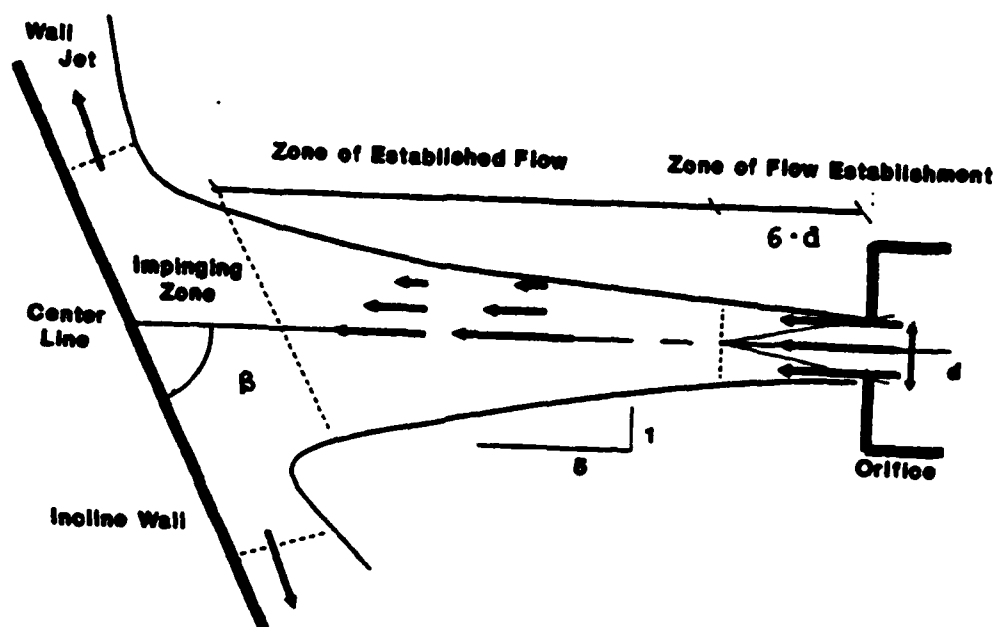


FIG. 5.-Submerged Radial Jet Mixing Diagram.

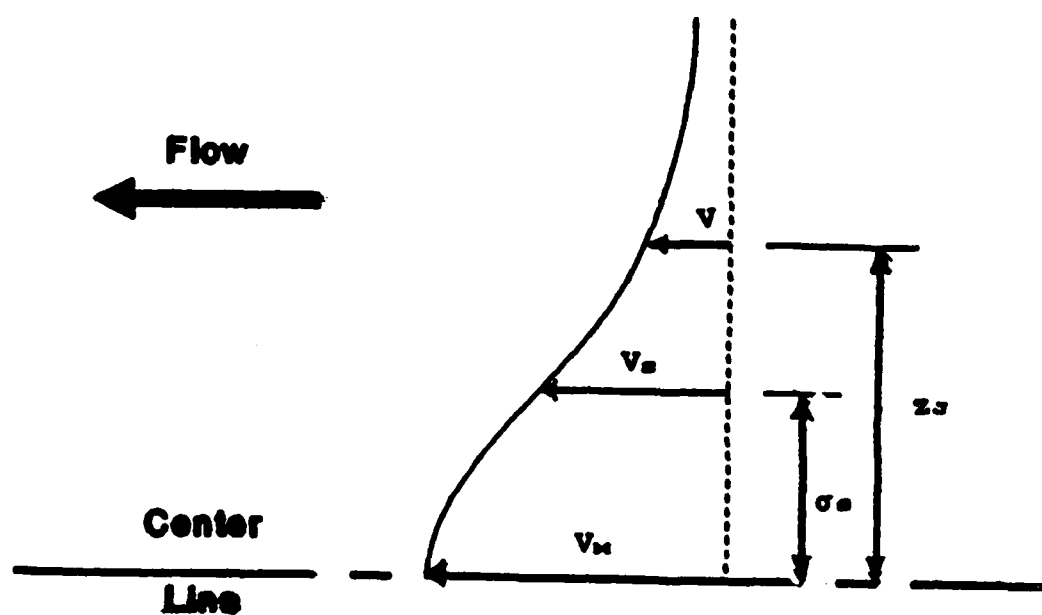


FIG. 6.-Normal Probability Curve of Radial Jet Mixing (Ref. 5 and 18).



$$E_M/E_0 = 4.1/(y_J/d) \dots\dots\dots (17)$$

where

$d$  = diameter of jet (ft),

$E_M$  = kinetic energy at a distance from the  
nozzle (ft-lb),

$E_0$  = initial kinetic energy at the nozzle (ft-lb),

$Q$  = volumetric flow rate at the nozzle (ft<sup>3</sup>/sec),

$Q_M$  = volumetric flow rate of entrainment at a  
distance from the nozzle (ft<sup>3</sup>/sec),

$V_0$  = jet velocity at nozzle (ft/sec), and

$y_J$  = distance from nozzle along center line (ft).

The impinging zone is the result of the translation of the impinging jet into the wall jet. The wall jet, as described by Glauert (11), is comprised of two zones. The outer zone is characterized by free turbulent flow, and the inner zone is dominated by the effects of the wall. Using Prandtl's model, Glauert was able to obtain solutions for both zones depending on a single parameter, and noted that the inner and outer velocities decrease at different constant rates with respect to outward radial distance. The outer velocity decreases more rapidly due to mixing with surrounding water at the boundary when compared to inner velocity which decreases due to shear along the wall boundary. Thus, the wall jet velocity profile will grow proportionately with respect to radial distance.

Glauert's experiment used a rigid, smooth and impervious boundary, but these conditions do not exist in the study of scour with its perpetually changing bed configuration. The changing boundary will greatly effect the characteristics of the wall jet. Kobus, Leister and Westrick's (15) experimental study of the effects of wall jet on the scour of noncohesive material confirm this.

## CHAPTER III

## DIMENSIONAL ANALYSIS

The following variables are significant in influencing scour of cohesive soils by an inclined submerged water jet

<u>Variable</u>		<u>Units</u>	<u>Dimensions</u>
d	Diameter of orifice	ft	L
I <sub>p</sub>	Plastic index	percent water content	-
t	Time duration of scour	sec	T
v	Volume of scour depression	ft <sup>3</sup>	L <sup>3</sup>
V <sub>o</sub>	Water velocity at orifice	ft/sec	L/T
z	Distance from orifice to initial test sample's surface	ft	L
β	Angle of inclination of jet	degree	-
ρ	Mass density of water	slug/ft <sup>3</sup>	M/L <sup>3</sup>
μ	Dynamic viscosity of water	lbs·sec/ft <sup>2</sup>	M/(L·T)
τ	Soil shear strength	lbs·ft <sup>2</sup>	M/(L·T <sup>2</sup> )
τ <sub>TR</sub>	Tractive shear stress	lbs·ft <sup>2</sup>	M/(L·T <sup>2</sup> )

Using the Buckingham pi theorem as described by Langhaar (16) and Olsen (21), z, μ and V<sub>o</sub> were designated as repeating variables. The Mass-Length-Time (MLT) System was used to produce the following eight pi terms from the eleven variables and three dimensions

$$\pi_1 = z/d$$

$$\pi_2 = v/d^3$$

$$\pi_3 = d \cdot \tau / (V_o \cdot \mu)$$

$$\pi_4 = d \cdot \tau_{TR} / (V_o \cdot \mu)$$

$$\pi_5 = d \cdot V_o \cdot p / \mu$$

$$\pi_5 = \beta$$

$$\pi_7 = I_p$$

$$\pi_8 = V_o \cdot t / d$$

Combining pi terms results in the following functional equation

$$f\{ z/d, v/d^3, d \cdot \tau / (V_o \cdot \mu), d \cdot \tau_{TR} / (V_o \cdot \mu), d \cdot V_o \cdot p / \mu, \beta, I_p, V_o \cdot t / d \} = 0 \quad \dots\dots\dots (18)$$

Since the Plastic Index,  $I_p$ , of the soil sample and water's mass density remained relatively constant throughout the experiment,  $d \cdot V_o \cdot p / \mu$  and  $I_p$  will be dropped as nonsignificant parameters. Also, since the tractive shear stress,  $\tau_{TR}$ , is difficult to determine, the normal center line stress on the initial sample surface as the result of jet,  $\sigma_J$ , will be substituted for the tractive shear leaving the following functional equation

$$v/d^3 = f\{ z/d, d \cdot \tau / (V_o \cdot \mu), d \cdot \sigma_J / (V_o \cdot \mu), \beta, V_o \cdot t / d \} = 0 \quad \dots\dots\dots (19)$$

A gravitational term was not included in the above functional equation since the soil sample will remain horizontal plane and the jet will be inclined. Thus, slope stability will be negated as a controlling parameter eliminating the requirement for a gravitational term.

Since a hypothesis of this experiment is that scour is related to the clay's shear strength and a logarithmic relationship exists between water content and shear strength of a sample as stated by Bowels (6),  $v/d^3$  will be divided by the water content,  $w_c$ , of the sample. This will reduce variance between samples of approximately

equal shear strength for comparison of the effects  $z/d$ ,  $d \cdot \sigma_s / (V_o \cdot \mu)$  and  $\beta$ . Eq. 19 can be modified to the following functional equation

$$v / (w \cdot d^3) = f \{ z/d, d \cdot \tau / (V_o \cdot \mu), d \cdot \sigma_s / (V_o \cdot \mu), \beta, V_o \cdot t/d \} = 0 \quad \dots\dots\dots (20)$$

Using the previously derived dimensionless pi terms and logic, the rate of scour, as described

<u>Variable</u>		<u>Units</u>	<u>Dimensions</u>
$Q_m$	Rate of Scour	ft <sup>3</sup> /sec	L <sup>3</sup> /T

will be substituted for the volume of scour,  $v$ . The resulting new  $\pi_2$  term is  $Q_m / (d^2 \cdot V_o)$  and Eq. 20 can be modified as follows

$$Q_m / (d^2 \cdot V_o) = f \{ z/d, d \cdot \tau / (V_o \cdot \mu), d \cdot \sigma_s / (V_o \cdot \mu), \beta, V_o \cdot t/d \} = 0 \quad \dots\dots\dots (21)$$

## CHAPTER IV

### EXPERIMENTAL APPARATUS AND EQUIPMENT

#### VANE SHEAR DEVICE

Soil analysis was performed in the Geotechnical Laboratory, Texas A&M University. Fig. 7 shows the laboratory vane shear device used to determine the clay's shear strength vs water content curve, and Fig. 8 shows the field vane shear device used to determine the clay's in situ shear strength.

#### CLAY

A clay with a trade name of Terra Cotta was used for this experiment. This clay was purchased from Trinity Ceramic Supply, Inc. of Dallas, Texas and is comprised of the following ingredients by percent weight:

<u>Percentage</u>	<u>Description</u>	<u>Primary Substances</u>
57.5%	Range Shale	SiO <sub>2</sub> , Al <sub>2</sub> O <sub>3</sub> , Fe <sub>2</sub> O <sub>3</sub>
24.8%	Dry Milled Fireclay	SiO <sub>2</sub> , Al <sub>2</sub> O <sub>3</sub>
7.8%	Soda Feldspar	SiO <sub>2</sub> , Al <sub>2</sub> O <sub>3</sub>
6.2%	Silica Crystal	
3.1%	Pyrophyll 100	
0.6%	Barium Carbonate	BaCO <sub>3</sub> + SrCO <sub>3</sub>

As prescribed by Bowels (6), the Atterberg Limits of the clay were determined and are presented in Fig. 9. The Atterberg Limits are

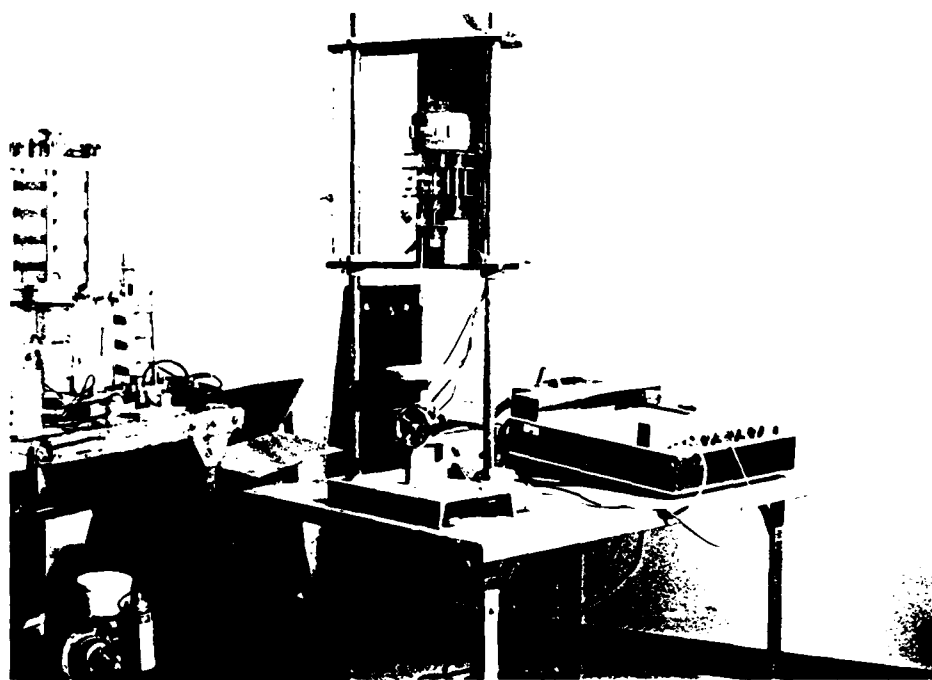


FIG. 7.-Laboratory Vane Shear Device.



FIG. 8-In Situ Vane Shear Device.

<u>Description</u>	<u>Percent Water Content</u>
Liquid Limit	37.0%
Plastic Limit	18.2%
Plastic Index	18.8%

Terra Cotta clay has an USCS classification of "CL" and a saturated unit weight of 110.0 pcf. The shear strength with respect to varying water content was determined using the laboratory vane shear apparatus as presented in Fig. 10.

The clay was pressed into 5.5 inch wide by 11.75 inch by 4.0 inch high brick-like samples weighing approximately 15 pounds. A Cinva Ram, as shown by Fig. 11, was used to press these blocks.

#### MODEL TEST

The model test consisted of three individual experiments conducted in the Hydromechanics Laboratories, Texas A&M University. All three experiments were performed in a 18 inch wide by 35 inch long by 21 inch deep static tank with an 18 inch high elevated drain to maintain a constant water elevation. Furthermore, all three utilized a turbulent, submerged and radial water jet created by an orifice, as shown by Fig. 12 and 13, with a discharge diameter of 3/16 inch.

The first part of the experiment centered on the study of clay scour. A clay sample was placed horizontally



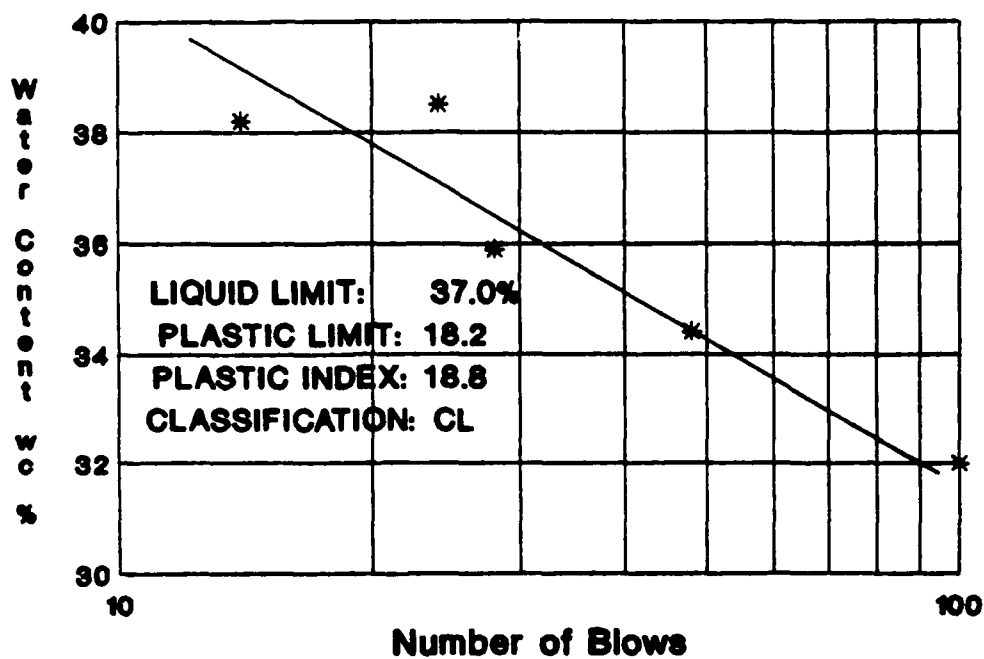


FIG. 9.-Atterberg Limit Results.

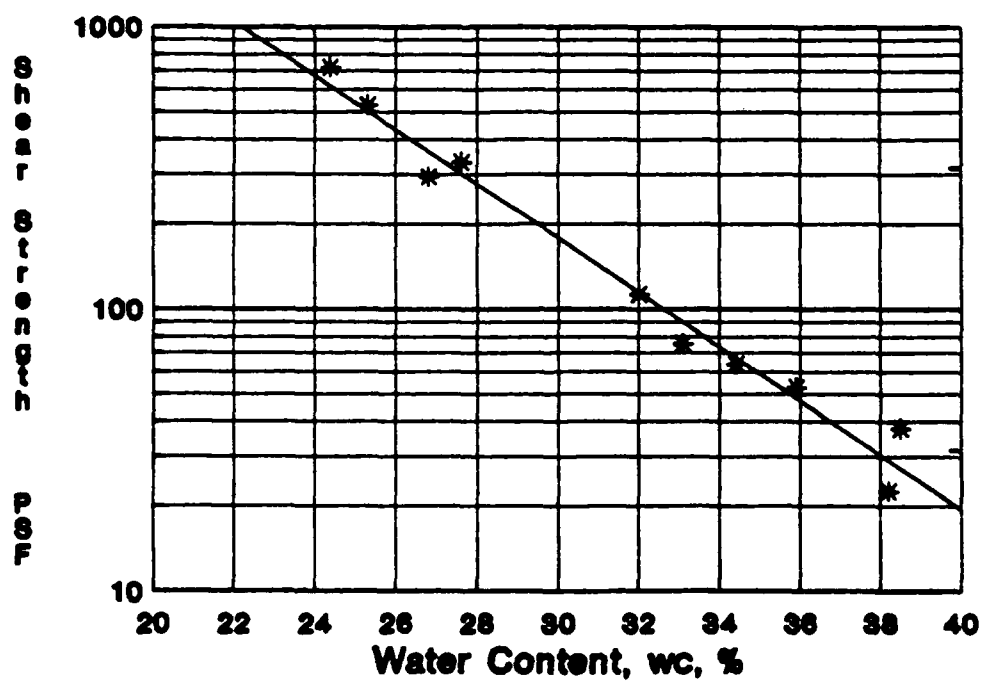


FIG. 10.-Vane Shear Strength vs Water Content Percentage.



FIG. 11.-Cinva Ram.



FIG. 12.-Orifice.

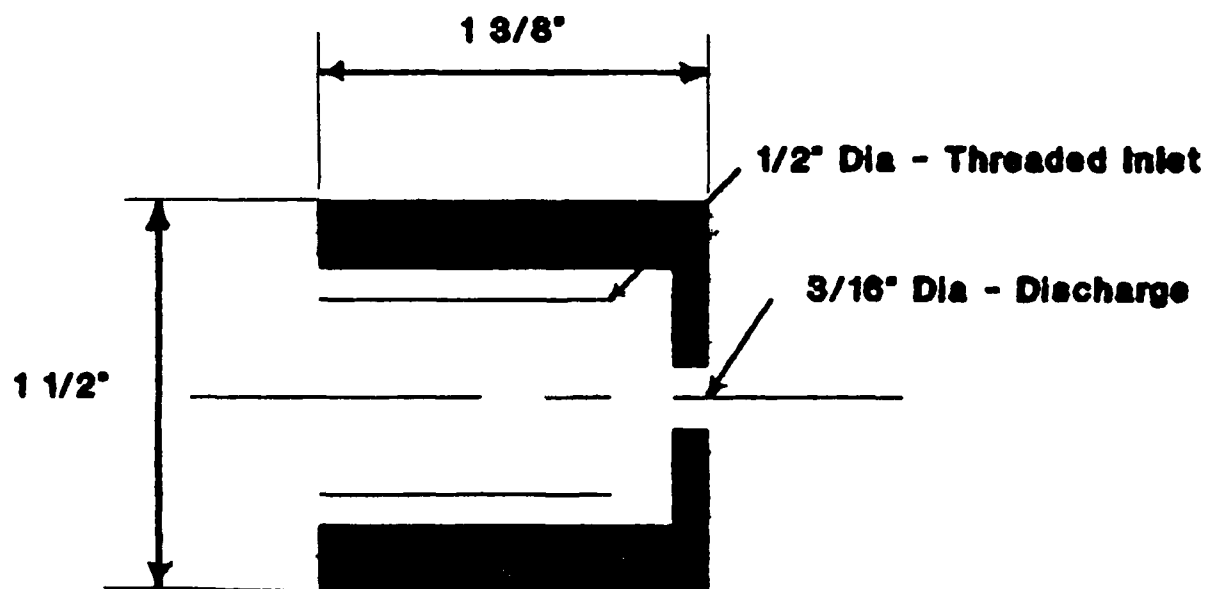


FIG. 13.-Orifice Sketch.

directly beneath the submerged jet, as shown by Figs. 14 and 15, and allowed to impinge upon it for three 5 minute time durations. The volume of eroded material was determined after completion of each duration. The jet's angle of inclination and distance from test sample was varied to achieve various test conditions.

Maintaining the sample's surface in the horizontal plane minimized the effect of gravity by negating slope stability. This allowed the experiment to focus on the mechanisms of scour.

The second part of the experiment was to determine the normal pressure distribution along the sample's surface due to the impinging jet's thrust. The clay sample was replaced with a 14 inch wide, 14 inch long and 6 inch high weighted, watertight plexiglass box with four pressure transducers imbedded in the box's surface as shown by Fig. 16. An integrating voltage meter was used to determine the voltage drop across the transducers and a additional voltage meter was used to monitor the direct current voltage source to the transducers as shown by Figs. 17 and 18.

The final part of the experiment was to determine the water jet's velocity profiles at given distances from the orifice. The vertically inclined jet was moved to the horizontal, and an anemometer was used to determine the velocity profiles as shown by Figs. 19 and 20. The hot film probe was secured to a carriage that permitted it to



FIG. 14.-Scour Apparatus.

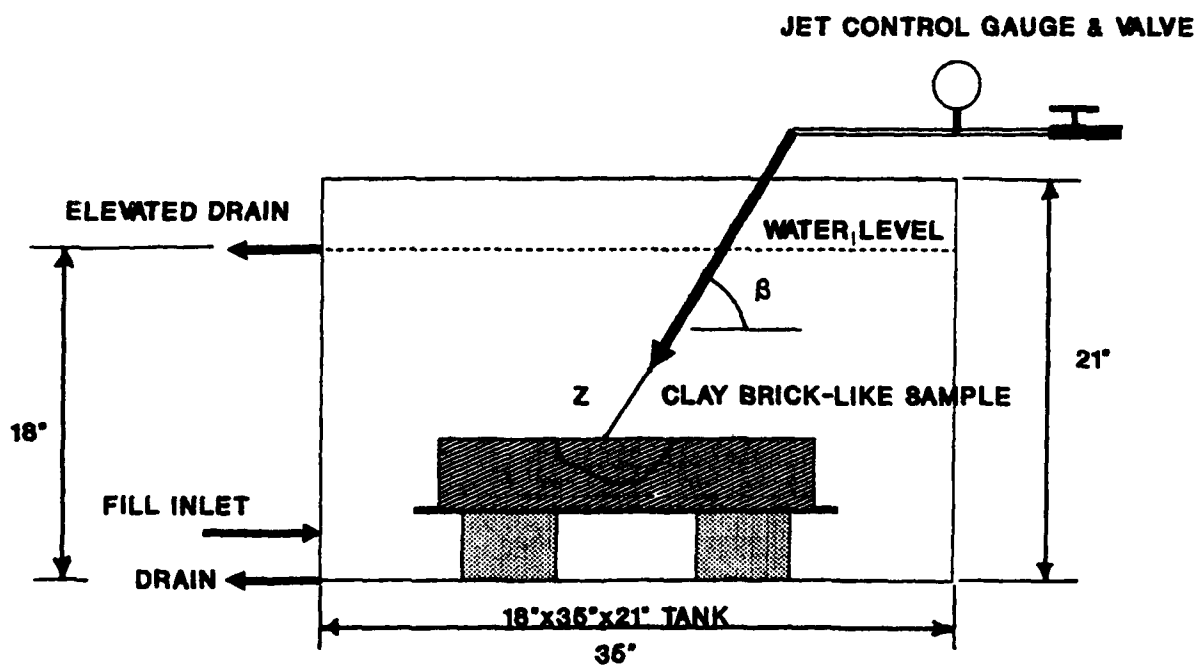


FIG. 15.-Scour Apparatus Sketch.

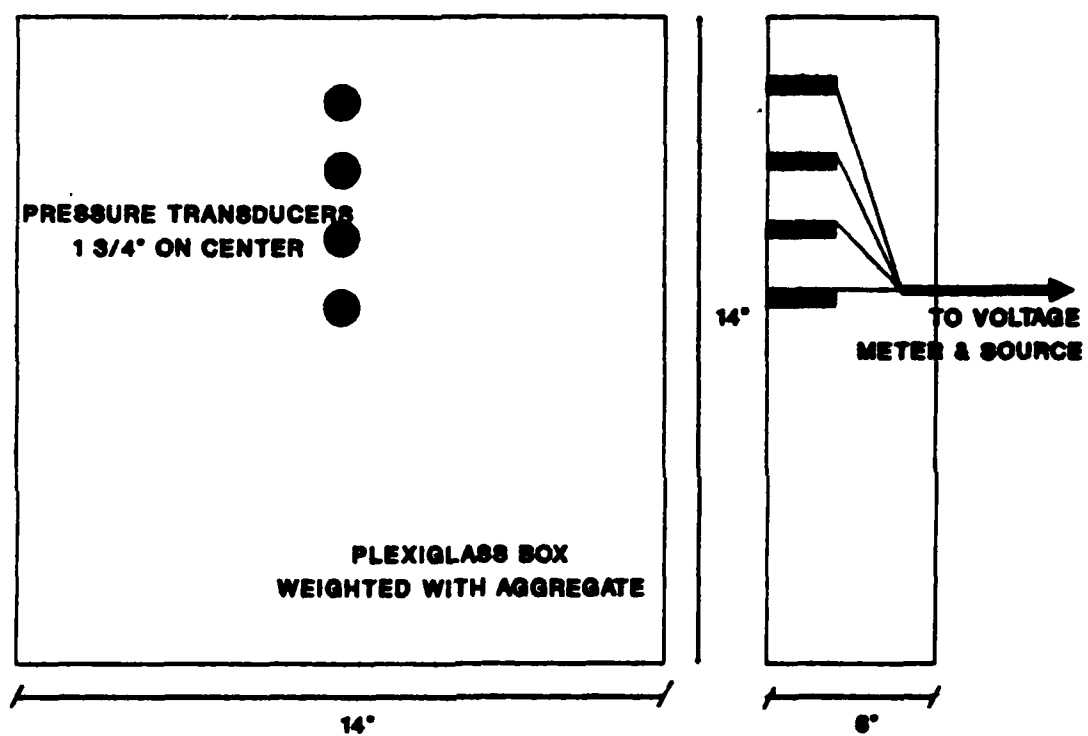


FIG. 16.-Pressure Transducer Box Sketch.

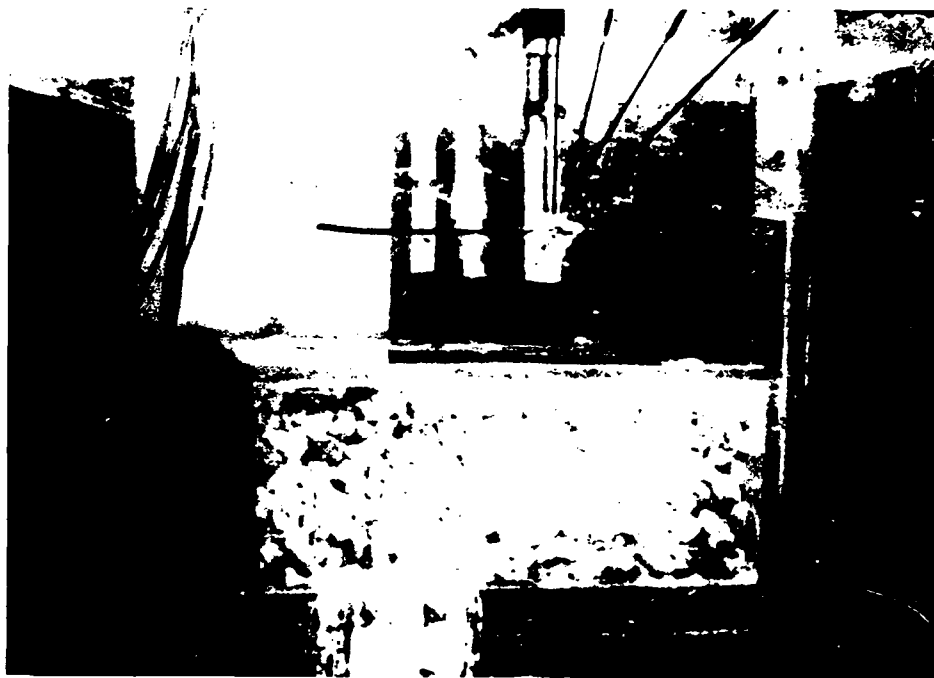


FIG. 17.-Thrust Apparatus.

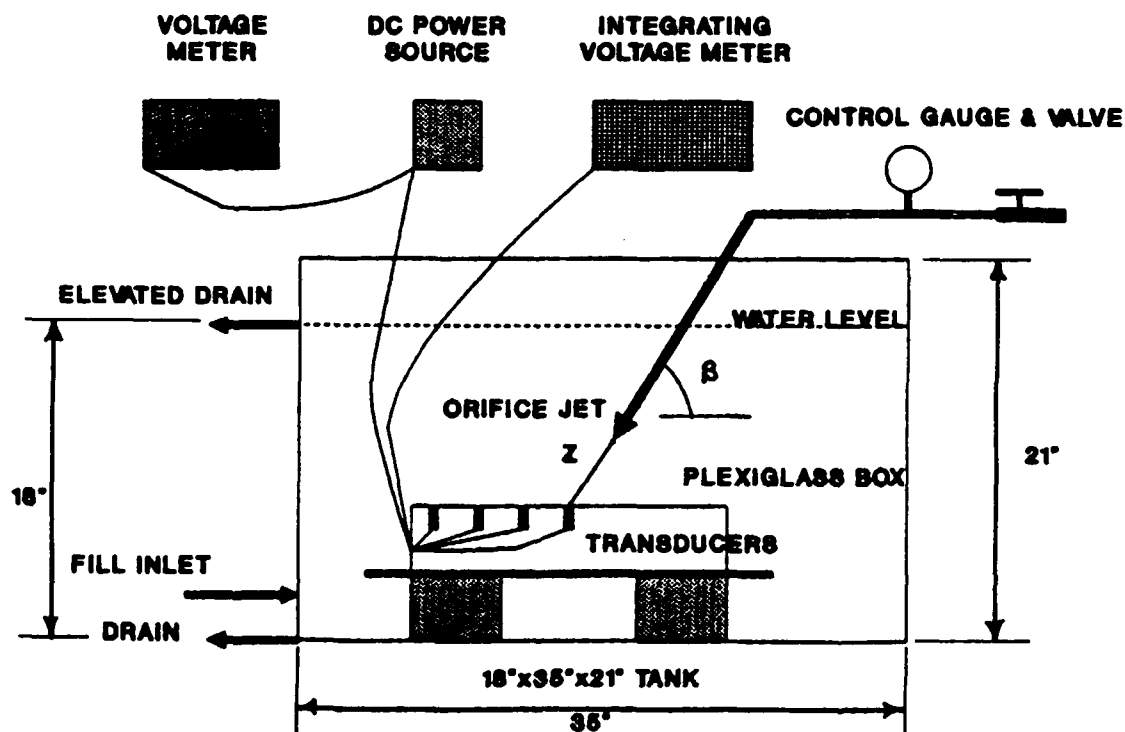


FIG. 18.-Thrust Apparatus Sketch.

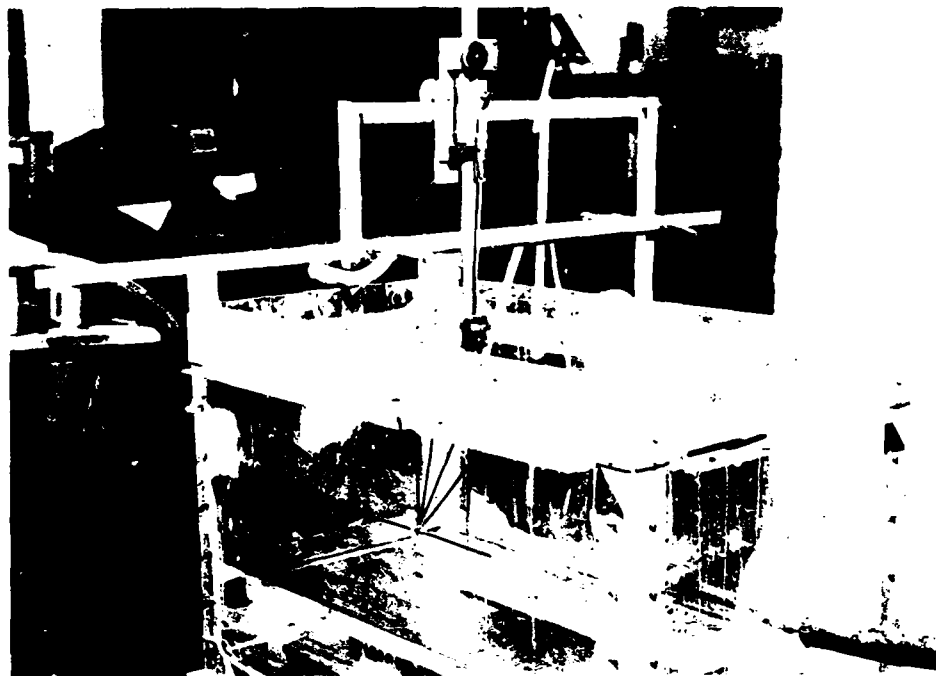


FIG. 19.-Velocity Apparatus.

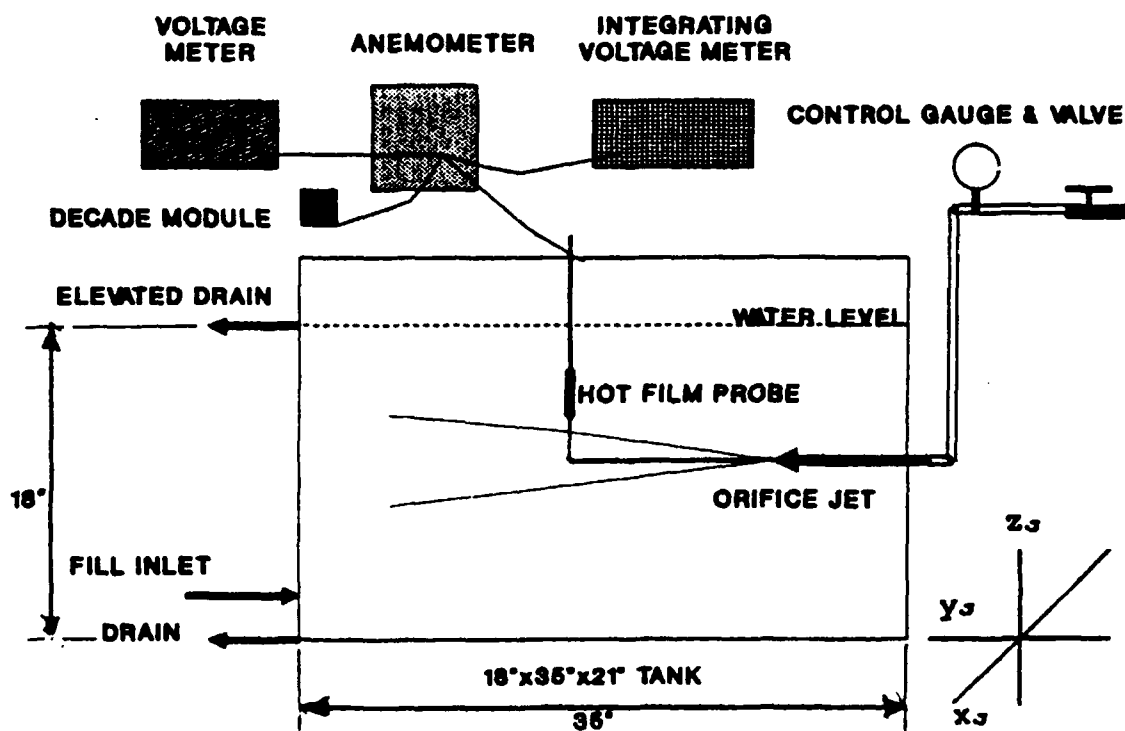


FIG. 20.-Velocity Apparatus Sketch.



be moved with respect to distance from the orifice along the jet's center line and cross the jet normal to the center line. The probe was attached to an anemometer which is comprised of a Wheatstone bridge and direct current voltage source. An integrating voltage meter was used to measure the output voltage and an other voltage meter was used to measure the input voltage of the Wheatstone bridge.

#### **WATER SOURCE**

The water source for the radial jet was the fresh water domestic supply. This water source was delivered to the experimental apparatus via a 0.75 inch water line which was reduced to 0.5 inch prior to reaching the orifice. The initial in-line head was 70 psi and water temperature was approximately 74° F.

The jet's discharge velocity from the orifice was regulated by a pair of pressure gauges and valves in series as shown by Fig. 21. The first pair, nearest the source, consisted of a gate valve that functioned as the "on/off switch" for the water supply followed by a pressure gauge to monitor any fluctuations in pressure of the source water supply. This pair was denoted the "main control" and was followed by another pair denoted the "jet control". The jet control consisted of a gate valve to regulate the water flow to the jet allowing the initial potential head to be reduced. A precision pressure gauge

followed the jet control valve to monitor the reduced water pressure allowing the maintenance of a constant water flow to the jet.

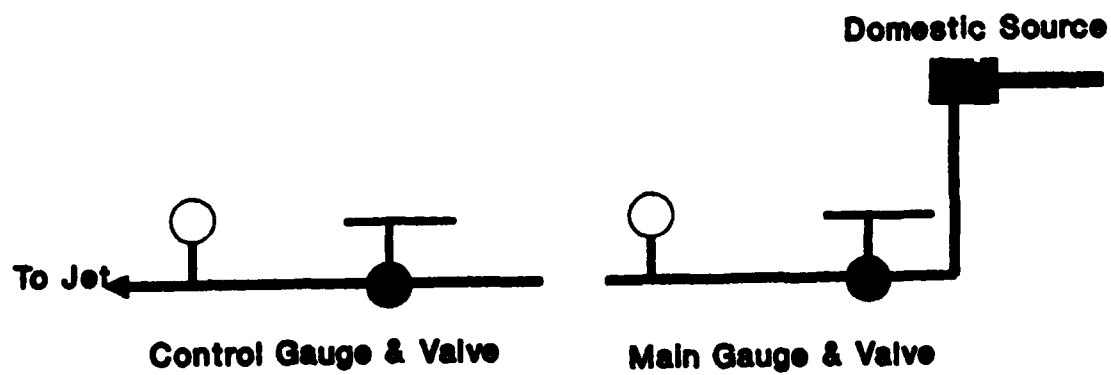


**FIG. 21.-Main and Control Valves.**

## CHAPTER V

### EXPERIMENTAL PROCEDURE

#### SAMPLE PREPARATION

The consistent preparation of the clay samples was critical in achieving coherent experimental results. Uniform water content throughout the sample was achieved by mixing the original manufactured clay, 26% water content, with a watered or dewatered clay in different portions to achieve the sample's new water content. Approximately 50 pounds of the original manufactured clay was placed in a mortar mixing trough and the appropriate amount of watered or dewatered clay was added. A concrete probe vibrator was used in a swirling motion to mix the clays together. Also, the clay on the outer edges of the trough was shoveled to the center during the mixing process to insure uniformity throughout the clay. Additional 50 pound batches of clay were added and mixed until the total batch reached 250 pounds. The in situ vane shear apparatus was used to determine the clay's shear strength which is a direct indicator of the clay's water content. Upon completion of the mixing process, the total batch was allowed to stand for a 24 hour period.

After the 24 hour period, the clay was pressed into blocks using a Cinva Ram to achieve consistent

consolidation. A 17 pound lump of clay was placed in the Cinva Ram and pressed uniformly into a 15 pound, 5.5 inch wide by 11.75 inch long, by 4 inch high block. The other 2 pounds were excreted from the Cinva Ram. The block was then placed back into the Cinva Ram on its side along with the excreted material and repressed. This was done to insure minimal air voids.

Immediately after pressing, three blocks were used to construct one sample. Two of the three were cut lengthwise to make four 2.75 inch wide by 11.75 inch long by 4 inch high blocks. These cut blocks were placed adjoining the four sides of the uncut block and uniformly pressed together using "C" clamps. The resulting sample was 10.5 inches wide by 16 inches long by 4 inches high as shown by Fig. 22.

#### SCOUR ANALYSIS

A sample of clay was placed in still water for 15 minutes. The sample did not show appreciable swell, but slight dispersion of the surface particles was noticed. Water slightly penetrated the surface and the surface became sticky to touch.

The experiment relating to scour is outlined in Table 1. The water content of various samples was varied with respect to different combinations of the jet's angle of inclination and distance from sample. The angles of inclination of the jet were 90° (vertical), 75°, 60° and

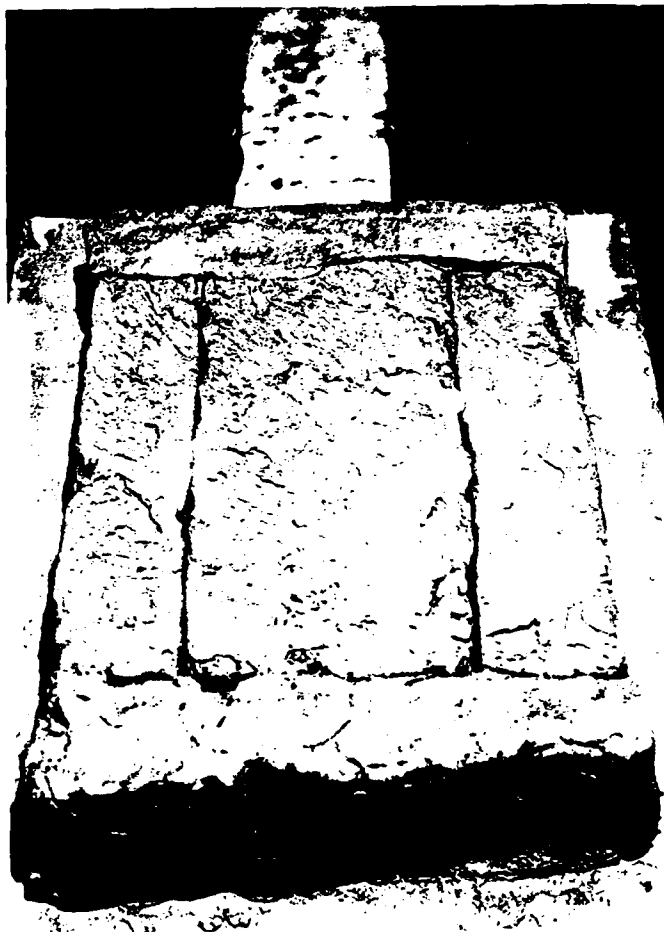


FIG. 22.-Clay Sample.

Table 1.- Test Program.

Sample Water Content WC (%)	Angle of Inclination $\beta$ (degree)			
	90°	75°	60°	45°
	Separation Distance Between Sample and Jet Inlet. z (inch)			
WC > 28.0%			z = 3.0 z = 2.5	
26.7% < WC > 27.3%	z = 4.0 z = 3.5 z = 3.0 z = 2.5	z = 3.5 z = 3.0 z = 2.5	z = 3.5 z = 3.0 z = 2.5	z = 3.5 z = 3.0 z = 2.5
WC < 26.6%		z = 3.0 z = 2.5	z = 3.0	z = 3.0 z = 2.5

45°. The primary distances between the orifice's discharge opening and samples' initial surface were 2.5, 3 and 3.5 inches.

Prior to placing a sample in the tank, the jet control gauge pressure was calibrated to 25 psi. This was done by filling the tank to the inlet of the elevated drain and opening the main control valve. The jet control valve was then used to adjust the jet control pressure. The jet control pressure was monitored continuously and adjusted to maintain a constant head.

Upon completion of calibrating the jet control pressure gauge, the main control valve was used to secure the water source and the tank was drained. A sample was then placed in the tank, and the orifice was positioned to the specified angle of inclination and distance. After filling the tank, the main control valve was opened to the precalibrated jet control pressure, and the jet was allowed to impinge upon the sample for a total time duration of 5 minutes. The tank was then drained; however, the scour depression retained its trapped water. The trapped water was removed and measured using a large surgical syringe to determine volume of scour material. This methodology was repeated for total time durations of 10 and 15 minutes, and the results for each sample are recorded in Appendix II.

Upon the completion of each test a representative sample of clay was taken to determine the water content of



the test sample. Also, various tests were photo-documented.

#### **JET THRUST ANALYSIS**

The clay sample was replaced with a plexiglass box with four pressure transducers imbedded into its surface. Each combination of the jet's angle of incline and distance, as specified by Table 1 for scour analysis, was duplicated. The jet control pressure remained 25 psi, and the normal pressure distribution along the surface due to the jet's thrust was recorded and is shown in Appendix III. Due to the limited number of pressure transducers, the plexiglass box was rotated 90° in the horizontal plane three times per test to achieve a symmetrical cross profile.

#### **JET VELOCITY ANALYSIS**

The submerged water jet was moved to the horizontal plane, and the 25 psi control pressure was reestablished. A hot film probe connected to an anemometer was used to determine the jet's cross sectional velocity profile at distances of 2, 3, 6, and 12 inches from the orifice discharge opening. The profiles are recorded in Appendix IV.

The flow rate was also verified by measuring the volumetric outflow of the elevated drain with respect to time. The results are recorded in Appendix IV.

## CHAPTER VI

### ANALYSIS OF RESULTS

#### JET VELOCITY

By visual inspection of the submerged horizontal jet used in the jet velocity analysis experiment, it was determined that the jet's characteristics were similar to those described in Chapter II. The zone of flow establishment was approximately 1 inch in length corresponding to its theoretical value of  $6 \cdot d$  as described by Albertson, et al. (3). Downstream from this zone a highly turbulent region occurred, the established flow zone. Also, the visible boundary of the jet flow in the established flow zone had an approximate 1 to 5 slope.

Since all of the velocity cross sectional profiles recorded during the jet velocity analysis experiment were in the established flow zone, Eq. 15 was used to approximate the initial discharge jet velocity,  $V_o$ . The results of these calculations are listed in Table 2. The average value of 37.5 ft/sec was taken to be  $V_o$  for the remainder of the experiment. Furthermore, this value was verified by comparison to the initial velocity calculated from the elevated drain outflow recorded in Appendix IV.

Eqs. 13 and 14 were used to verify the normal distribution of the cross sectional velocity profile. Fig. 23 shows the comparison between theoretical

TABLE 2.-Initial Velocity of Jet.

Distance from Orifice $y_j$ (ft)	Center Line Velocity $V_m$ (ft/sec)	Initial Velocity at Orifice $V_o$ (ft/sec)
0.166	20.44	35.16
0.25	14.29	36.87
0.50	6.69	34.50
1.00	4.18	43.14
		37.5 Average

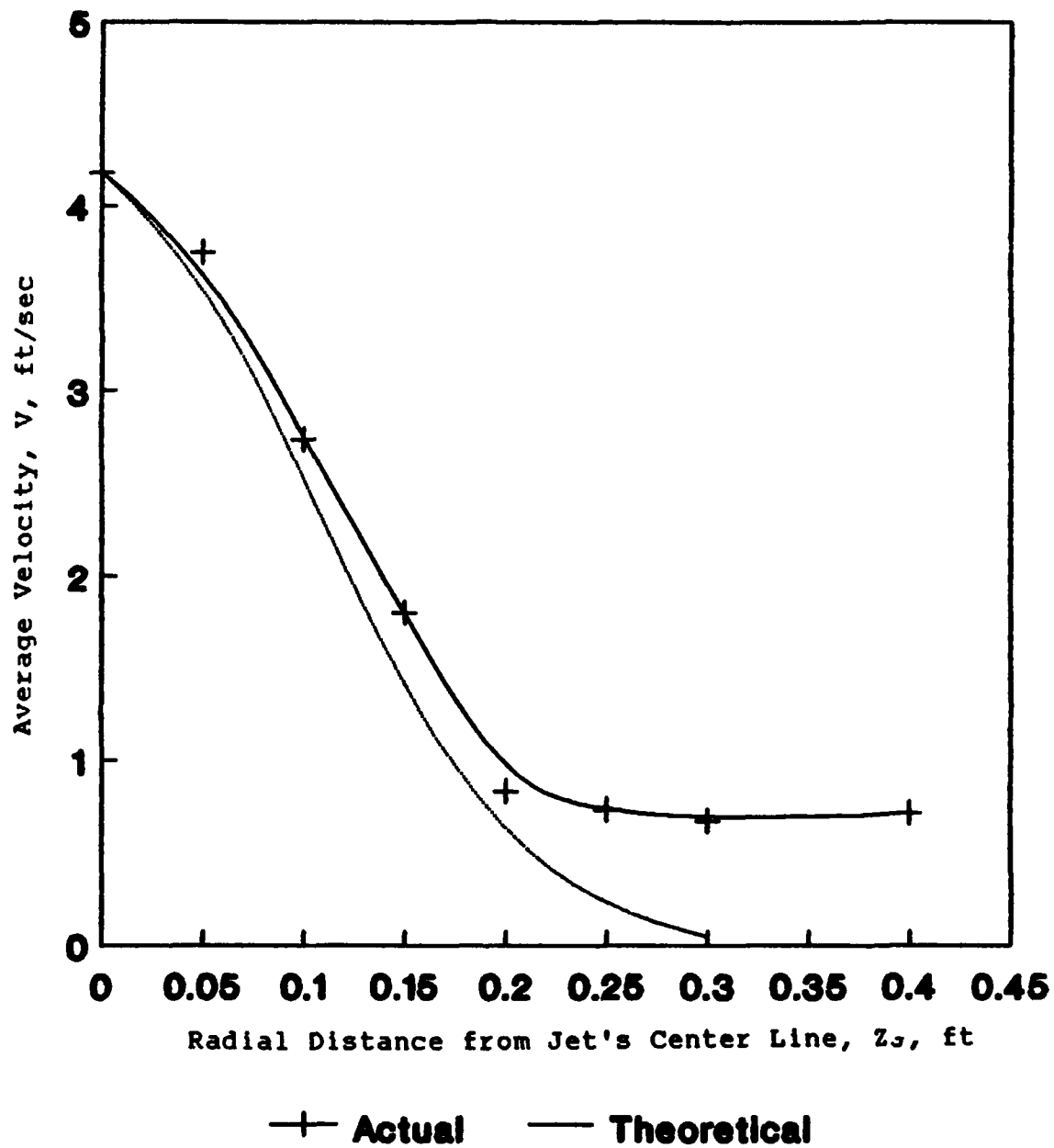


FIG. 23.—Normal Distribution of Jet.  $y_j = 1.0$  ft.

and actual velocity distributions of the cross sectional profile taken at  $y$ , equals 1.0 feet.

The variations and inconsistencies of the recorded velocities were caused by fluctuations of the anemometer output voltage. Possible causes for these fluctuations were: the voltage output was non-linearized, and the variable decade box used was inductive and did not possess the required precision. Also, turbulent boundary conditions resulting from the small tank size caused the outer cross sectional velocities to exist when none were expected.

#### JET THRUST

The normal pressure on the sample's surface resulting from jet thrust, as recorded by the center line pressure transducer,  $\sigma_j$ , decreased with respect to decreasing angle of inclinations and increasing distances from the sample's surface to the orifice's outlet as shown by Fig. 24. This was expected since decreasing the angle of inclination caused the impinging zone to assume an asymmetrical elliptical cross section. This allowed for a more efficient translation of the impinging jet to the wall jet reducing the center line normal pressure. Also, as predicted by Eq. 17 the kinetic energy of the jet decreased with increasing distance away from the orifice. Thus, the normal surface pressure will decrease accordingly.

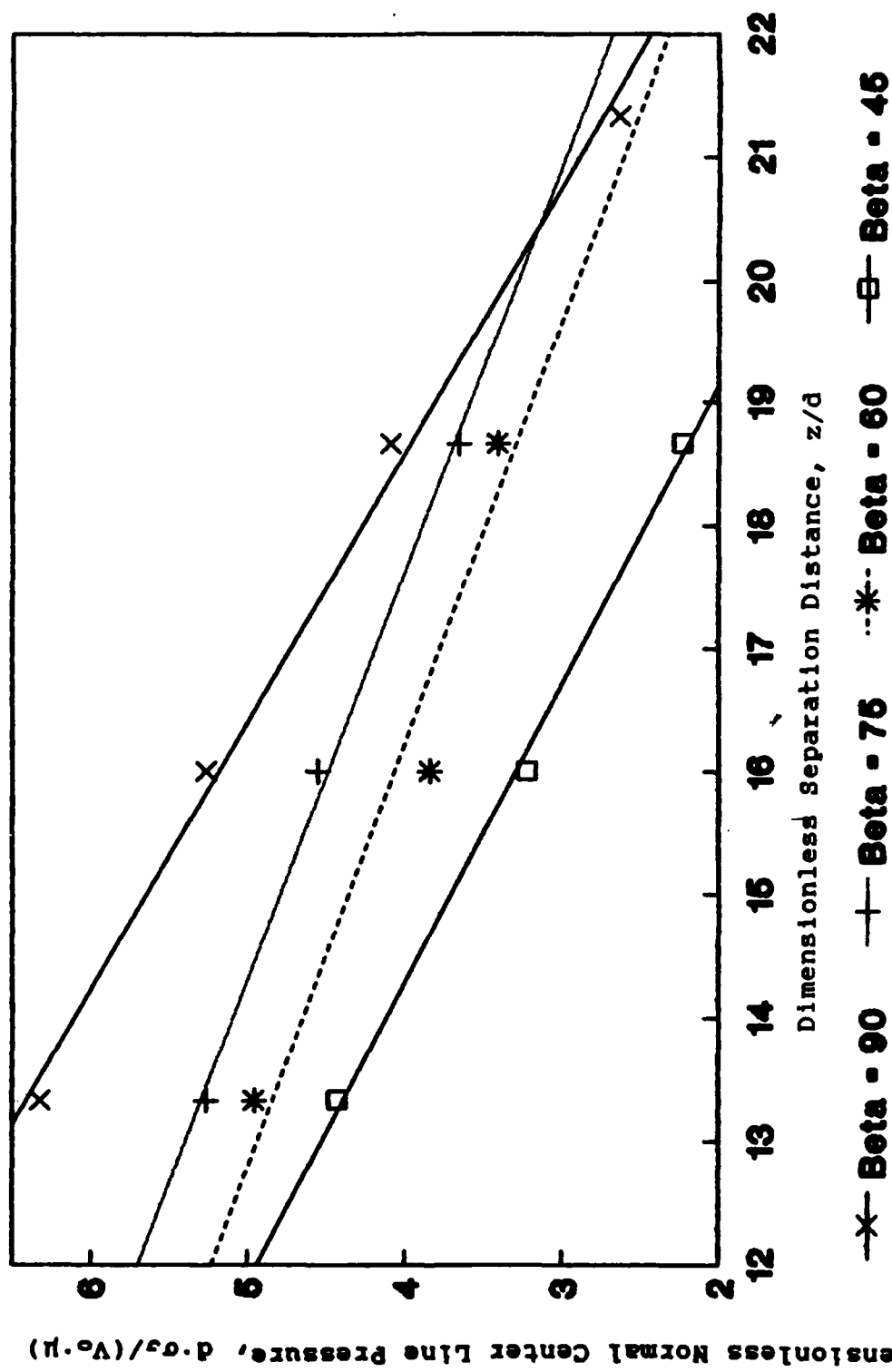


FIG. 24. Dimensionless Normal Center Line Pressure Resulting from Jet Thrust vs Distance of Separation.

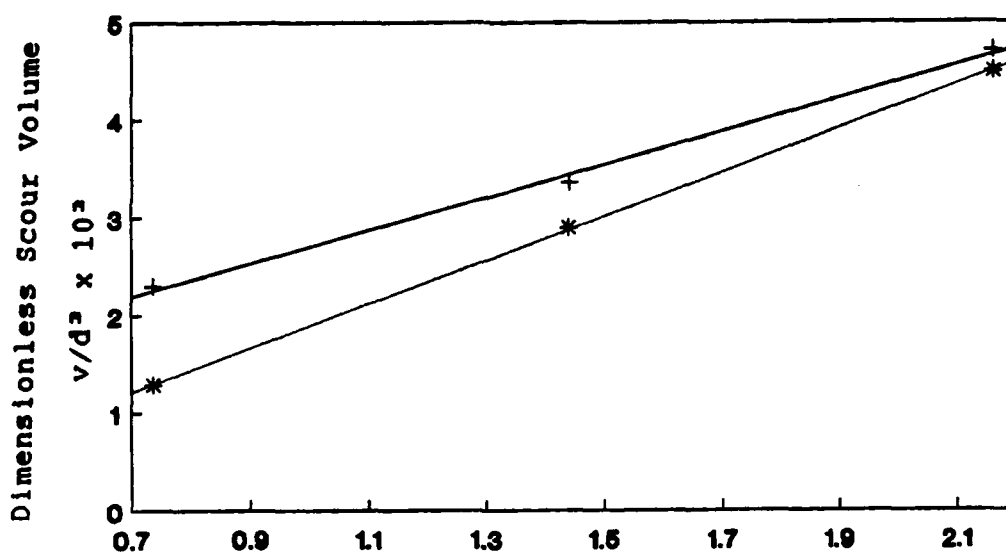
The jet's thrust profile was extremely narrow and the majority of the thrust was concentrated on the center line pressure transducer. As a result, the outer pressure transducers recorded no or little normal pressure.

#### SCOUR VOLUME

The critical tractive shear for Terra Cotta clay with a water content of 27.0% was calculated to be 1.1 psf using Eq. 1. In all of the tests the tractive shear force resulting from the jet thrust was greater than the clay's critical tractive shear and scour was initiated.

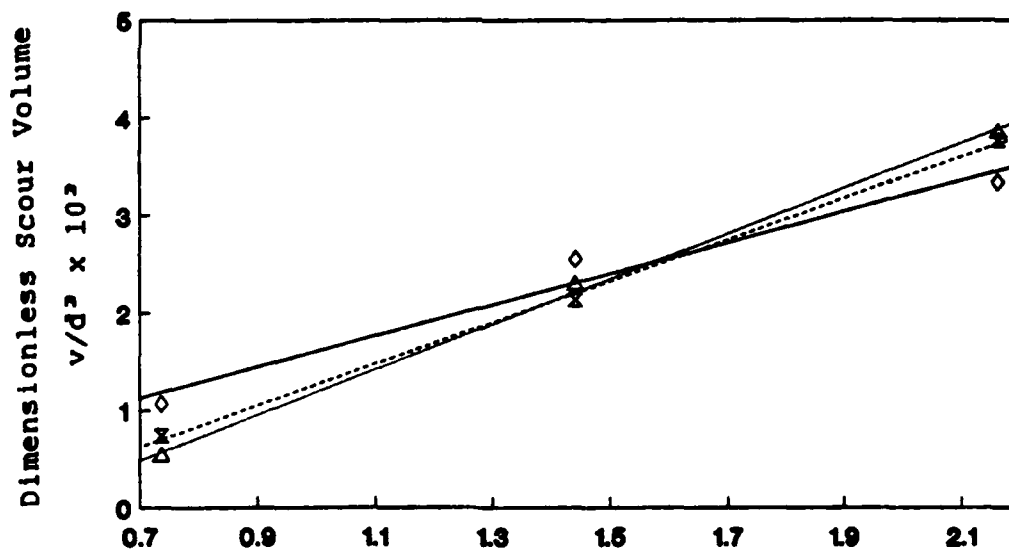
The experiment showed two mechanisms of scour. During the high tractive stress periods, the primary mechanism of scour was the detachment and removal of flat aggregate-like soil masses up to 1/4 inch thick. However, during the low tractive stress periods, the primary mechanism was particle-by-particle scour as indicated by the cloudiness of the water in the tank.

The  $\pi$  terms, developed in Chapter III for scour volume, were calculated and their interdependencies were studied. Figs. 25 through 48 were plotted and show these interdependencies. Figs. 25 through 42 show that the volume of scoured material is linearly related to the time duration of impingement for the time period of 5 to 15 minutes. If a one to one relationship is assumed between depth of scour and volume of scour, this relationship is contrary to Masch and Moore (19), and Abdel-Rahmann's (1)



Dimensionless Time of Impingement,  $V_0 \cdot t/d \times 10^6$

FIG. 25.-Dimensionless Scour Volume vs Time.  
 $\beta = 90^\circ$  and  $z/d = 13.33$ .



Dimensionless Time of Impingement,  $V_0 \cdot t/d \times 10^6$

FIG. 26.-Dimensionless Scour Volume vs Time.  
 $\beta = 90^\circ$  and  $z/d = 16.00$ .

Sample	wc	Sample	wc
+ B-I	26.8%	◆ B-I	27.1%
* B-II	26.7%	▲ B-II	27.1%
		⦿ B-III	27.1%



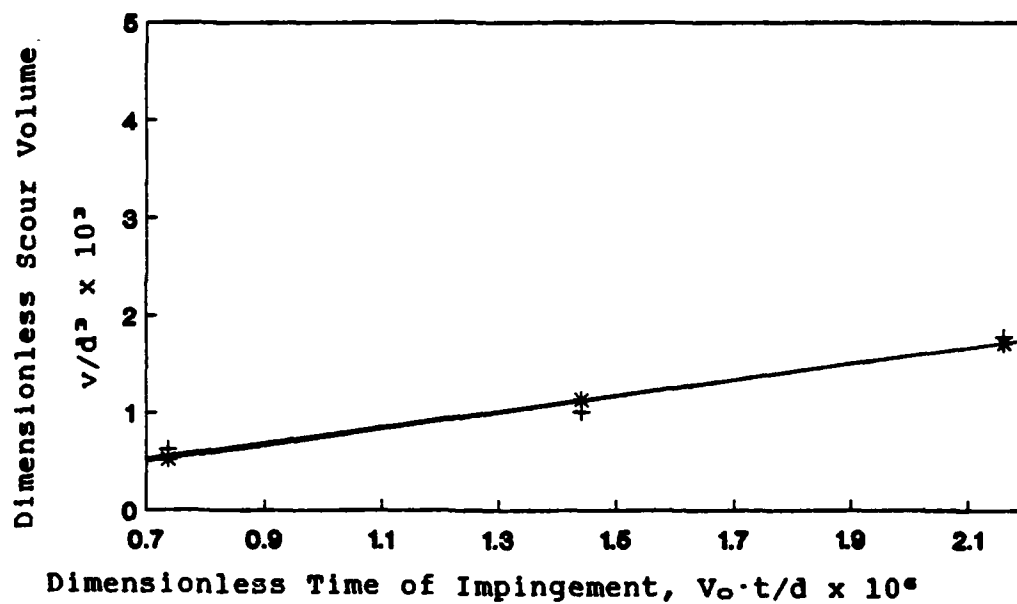


FIG. 27.-Dimensionless Scour Volume vs Time.  
 $\beta = 90^\circ$  and  $z/d = 18.66$ .

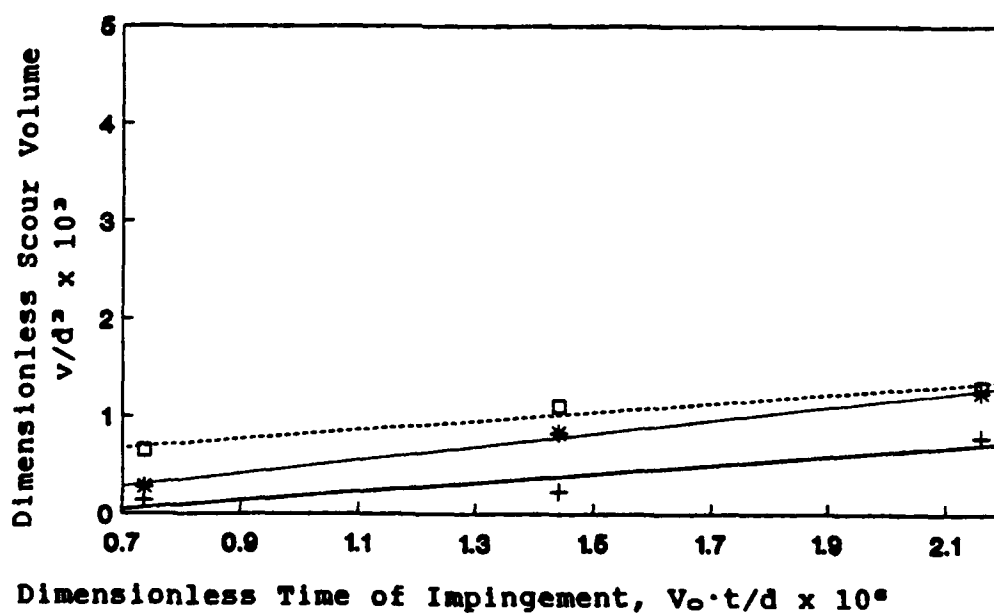
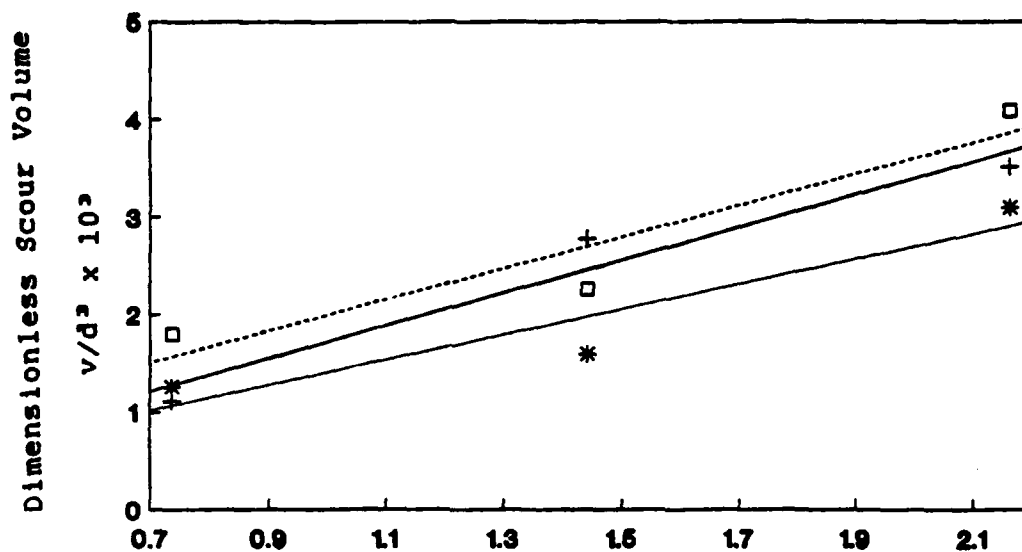


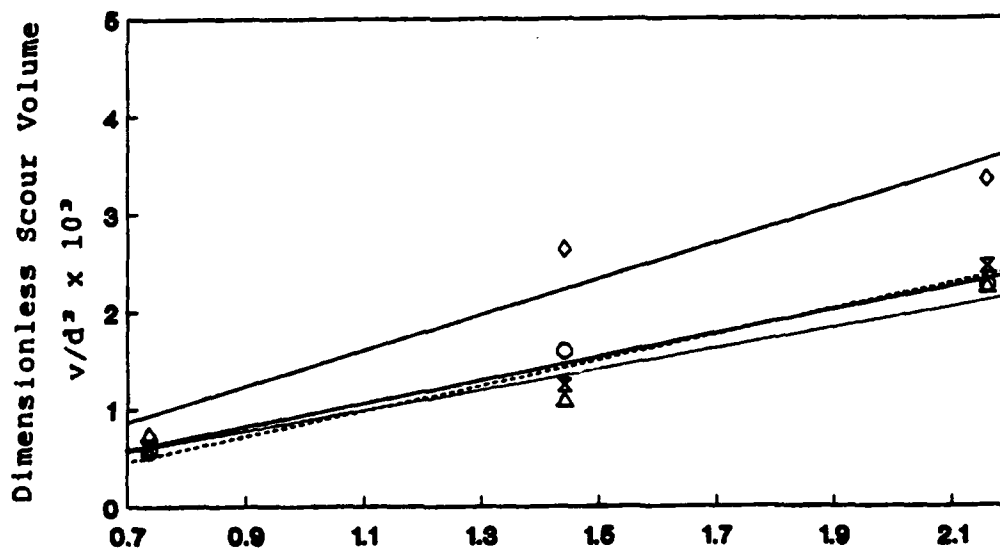
FIG. 28.-Dimensionless Scour Volume vs Time.  
 $\beta = 90^\circ$  and  $z/d = 21.33$ .

Sample	wc	Sample	wc
—●— B-I	27.1%	—●— B-I	27.0%
—+— B-II	27.2%	—+— B-II	27.1%
—*— B-III		—*— B-III	27.2%



Dimensionless Time of Impingement,  $V_0 \cdot t/d \times 10^4$

FIG. 29.-Dimensionless Scour Volume vs Time.  
 $\beta = 75^\circ$  and  $z/d = 13.33$ .



Dimensionless Time of Impingement,  $V_0 \cdot t/d \times 10^4$

FIG. 30.-Dimensionless Scour Volume vs Time. I of II.  
 $\beta = 75^\circ$  and  $z/d = 16.00$ .

Sample	wc	Sample	wc	Sample	wc
+ B-I	26.5%	◆ B-I	26.8%	◊ B-IV	26.2%
+ B-II	26.7%	▲ B-II	26.8%		
+ B-III	26.7%	■ B-III	26.8%		

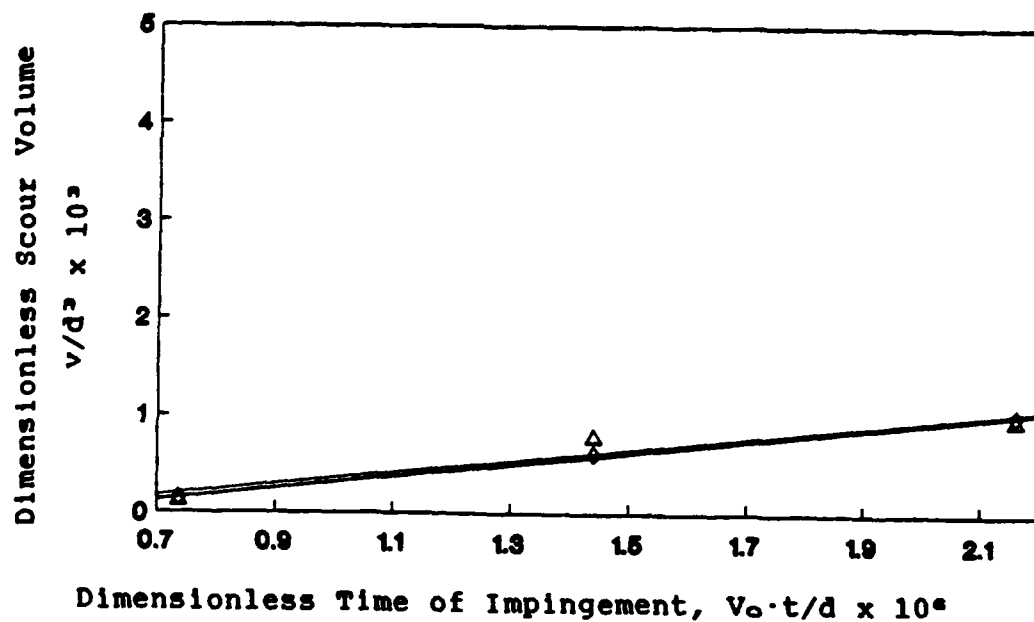
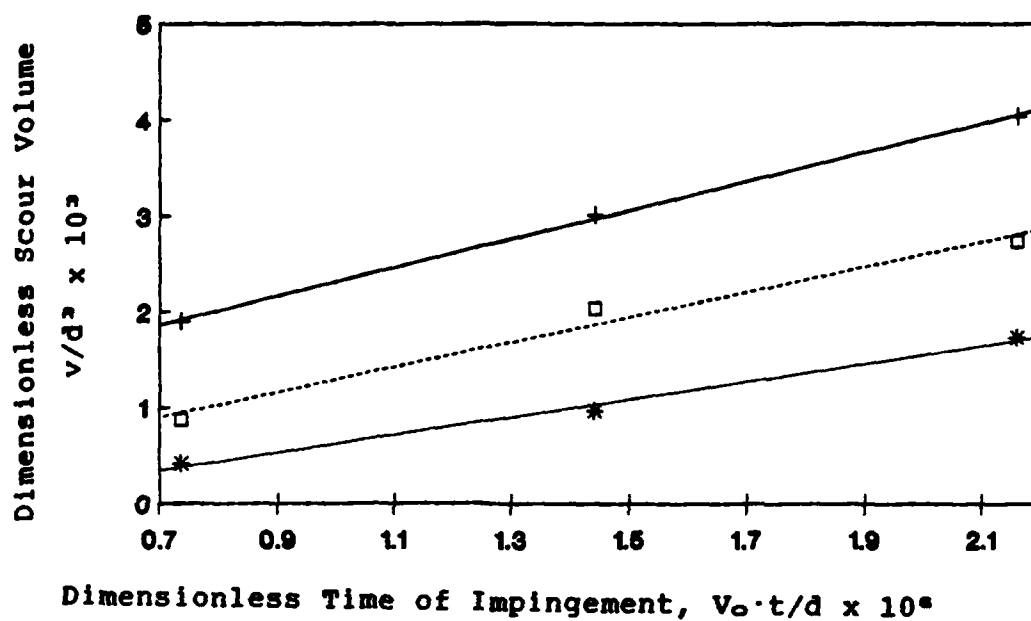
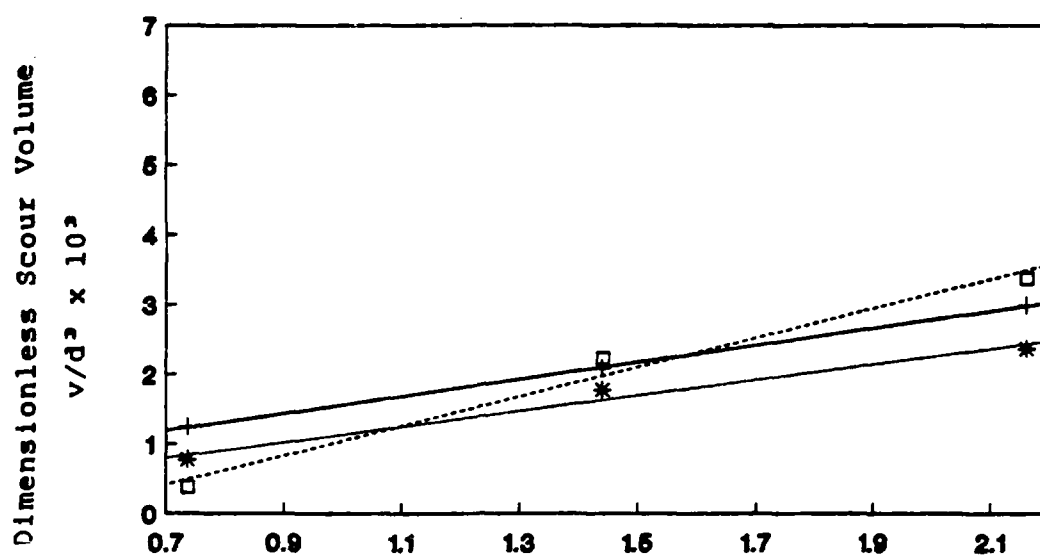


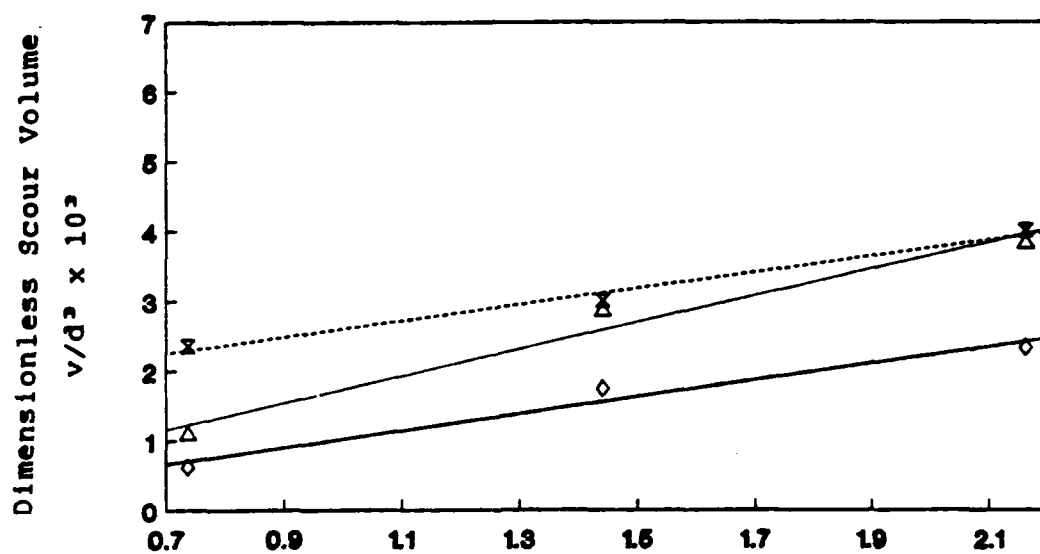
FIG. 32.-Dimensionless Scour Volume vs Time.  
 $\beta = 75^\circ$  and  $z/d = 18.66$ .

Sample	wc	Sample	wc
□ C-I	28.3%	● B-I	26.8%
* E-I	26.5%	▲ B-II	26.8%
+ G-I	27.0%		



Dimensionless Time of Impingement,  $V_0 \cdot t/d \times 10^6$

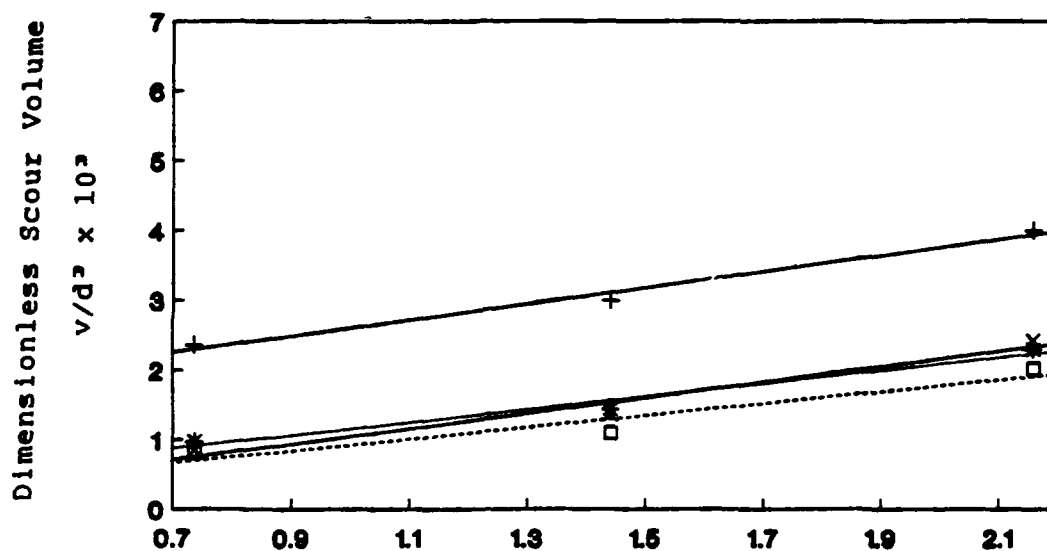
FIG. 33.-Dimensionless Scour Volume vs Time. I of IV.  
 $\beta = 60^\circ$  and  $z/d = 13.33$ .



Dimensionless Time of Impingement,  $V_0 \cdot t/d \times 10^6$

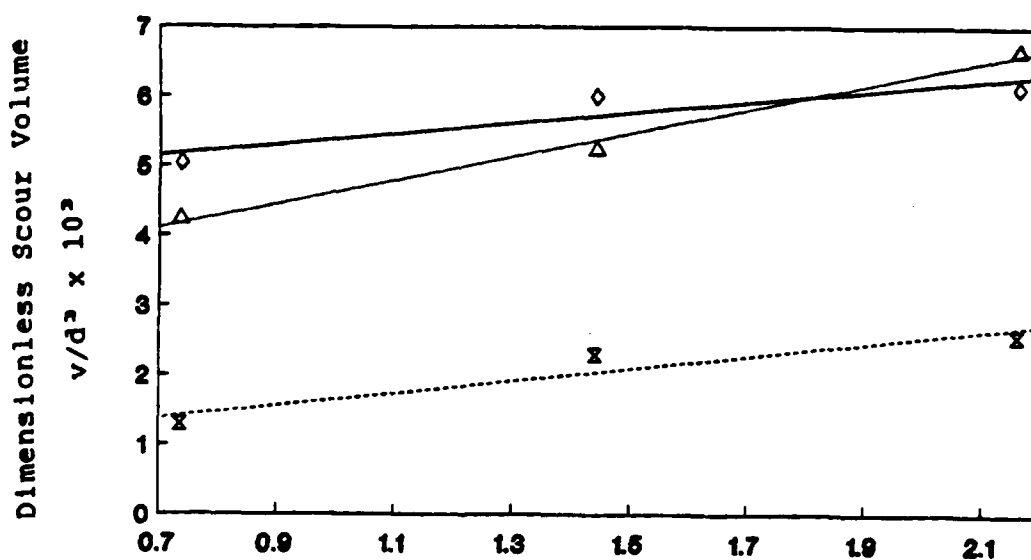
FIG. 34.-Dimensionless Scour Volume vs Time. II of IV.  
 $\beta = 60^\circ$  and  $z/d = 13.33$ .

Sample	wc	Sample	wc
—+— A-I	27.5%	—◆— B-II	27.2%
—*— A-II	27.3%	—△— C-I	27.9%
—□— B-I	27.0%	—×— C-II	28.1%



Dimensionless Time of Impingement,  $V_0 \cdot t/d \times 10^6$

FIG. 35.-Dimensionless Scour Volume vs Time. III of IV.  
 $\beta = 60^\circ$  and  $z/d = 13.33$ .



Dimensionless Time of Impingement,  $V_0 \cdot t/d \times 10^6$

FIG. 36.-Dimensionless Scour Volume vs Time. IV of IV.  
 $\beta = 60^\circ$  and  $z/d = 13.33$ .

Sample	wc	Sample	wc	Sample	wc
D-I	27.2%	E-I	27.5%	F-I	29.4%
D-II	27.5%			F-II	29.2%
E-I	27.2%			G-I	27.4%

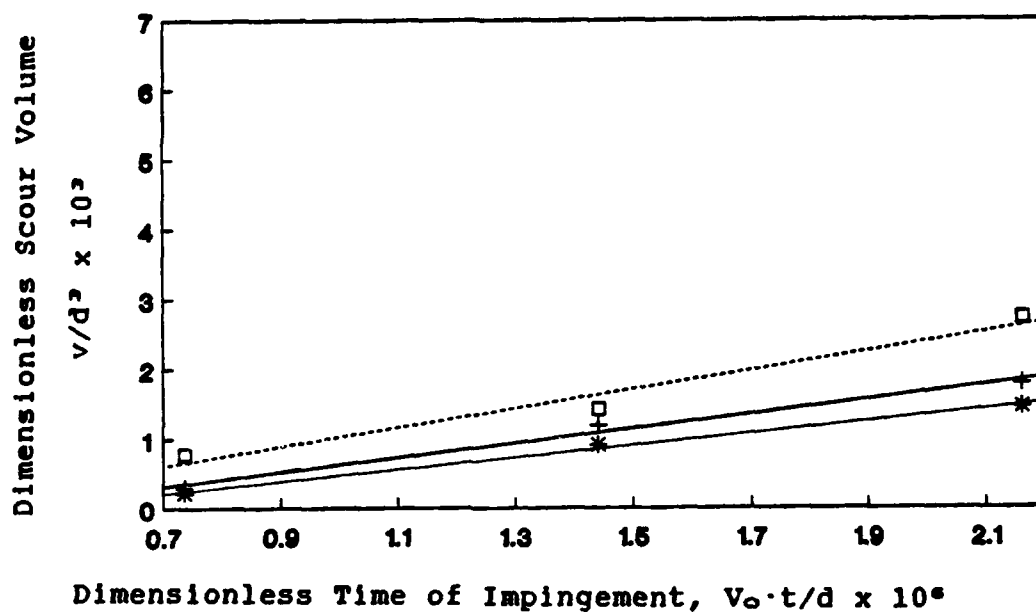


FIG. 37.-Dimensionless Scour Volume vs Time. I of II.  
 $\beta = 60^\circ$  and  $z/d = 16.00$ .

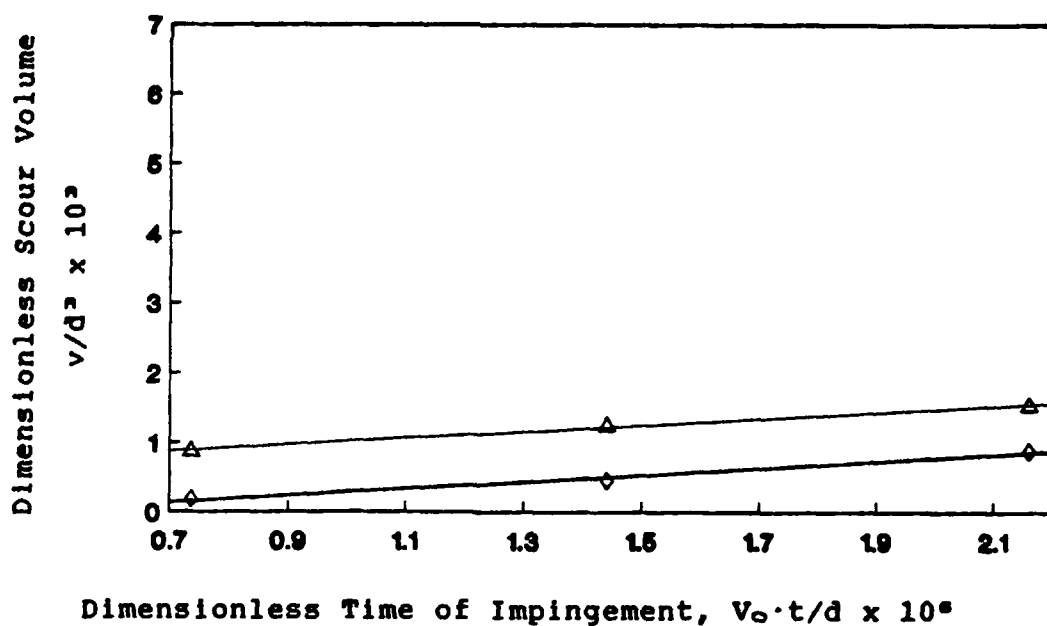
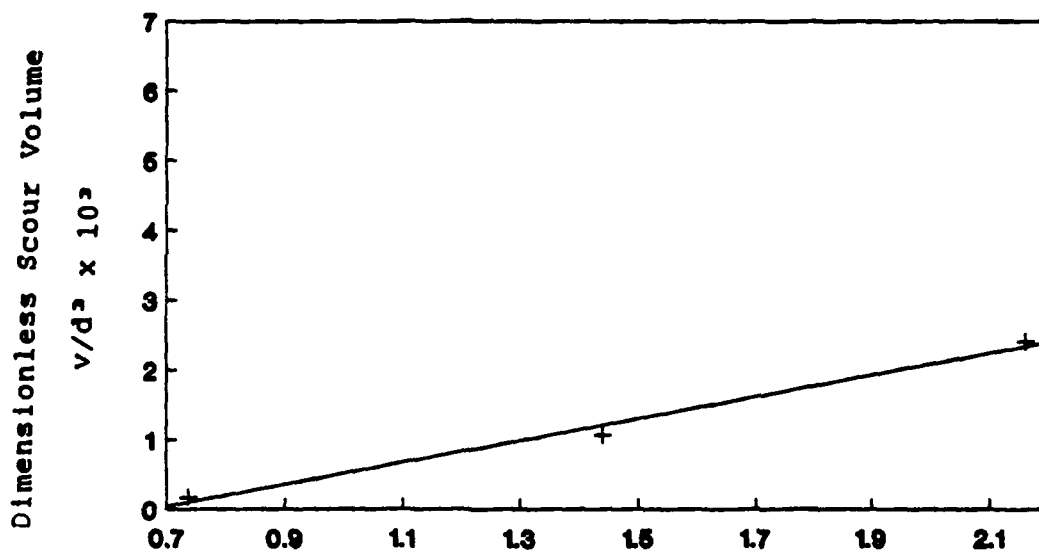


FIG. 38.-Dimensionless Scour Volume vs Time. II of II.  
 $\beta = 60^\circ$  and  $z/d = 16.00$ .

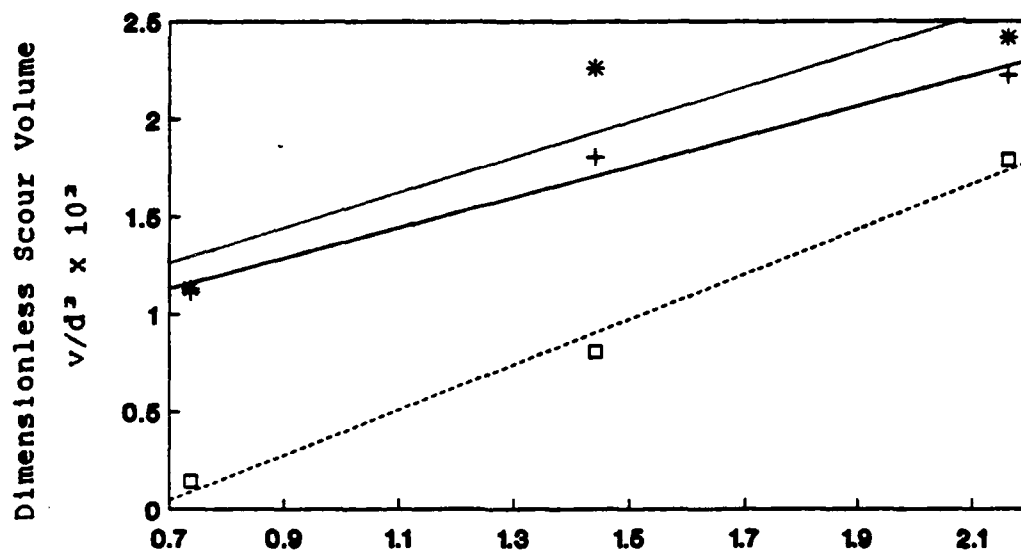
Sample	wc	Sample	wc
+ B-I	26.9%	◆ E-I	26.6%
* B-II	26.8%	▲ G-I	27.4%
□ C-I	29.0%		



Dimensionless Time of Impingement,  $V_0 \cdot t/d \times 10^4$

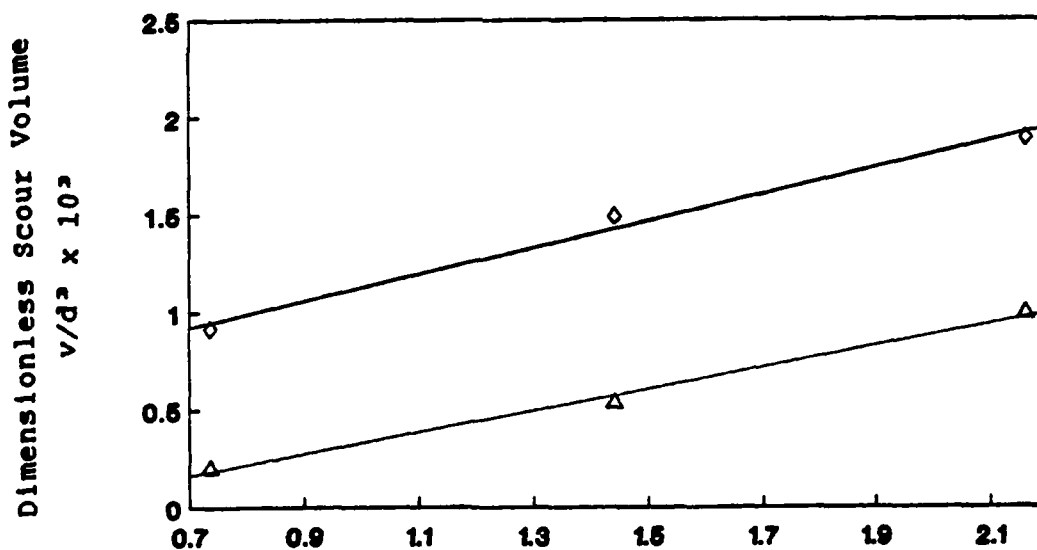
FIG. 39.-Dimensionless Scour Volume vs Time.  
 $\beta = 60^\circ$  and  $z/d = 18.66$ .

	Sample	wc
+	B-I	26.8%



Dimensionless Time of Impingement,  $V_0 \cdot t/d \times 10^6$

FIG. 40.-Dimensionless Scour Volume vs Time.  
 $\beta = 45^\circ$  and  $z/d = 13.33$ .



Dimensionless Time of Impingement,  $V_0 \cdot t/d \times 10^6$

FIG. 41.-Dimensionless Scour Volume vs Time.  
 $\beta = 45^\circ$  and  $z/d = 16.00$ .

Sample	wc
B-I	26.9%
B-II	26.9%
H-I	25.2%

Sample	wc
B-I	26.8%
H-II	25.3%



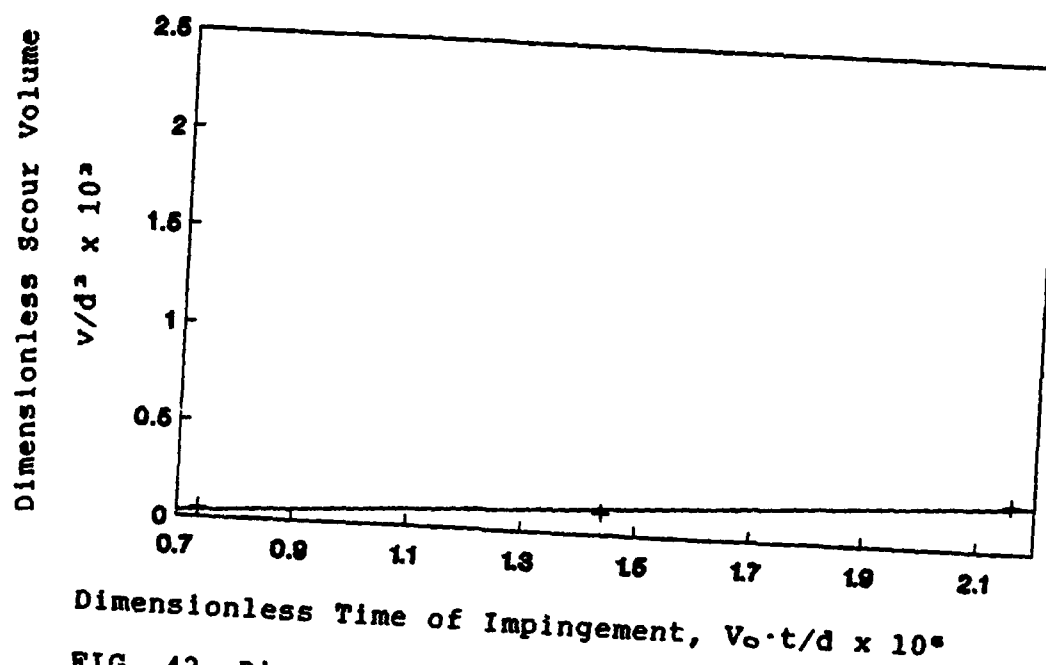


FIG. 42.-Dimensionless Scour Volume vs Time.  
 $\beta = 45^\circ$  and  $z/d = 18.66$ .

Sample	wc
+ B-I	26.8%

findings. They stated the depth of scour was logarithmically related to duration. The reason for these differing relationships might be that the duration of impingement used in this experiment was not sufficient to develop equilibrium scour conditions. The volume of scour with respect to time of impingement would decrease as equilibrium scour conditions were achieved causing a non-linear relationship. Furthermore, the time increments between scour volume measurements might have been too large to record the initial non-linear period of scour. The linear relationships calculated using least squares estimates for Figs. 25 through 42 should pass through the origin since no scour occurred at time zero. However, this is not the case for the majority of samples tested indicating that an exponentially shaped curve would be representative of the initial scour until the linear relationship was established. Thus, the duration of impingement with respect to scour volume recorded during this experiment may not be representative of the entire scour cycle.

Also, Figs. 25 through 42 show a relationship between the shear strength of clay and volume of scour as described by Abt, Ruff, and Shaikh (2) and Bhasin, Lovell, and Toebe (5). A sample containing a high water content, low shear strength, had a greater scour volume than a sample containing a low water content, high shear strength. This is most evident in the extremes, a sample

with a water content above 28% or below 26.5%, when compared to a sample containing 27% water content. However, a distribution of scour volumes can be observed for samples consisting of the same water content. This indicates that the shear strength/volume of scour relationship is not a strong one, or since scour is a natural phenomenon the scour volume might assume a normal distribution curve about a given shear strength.

Since a relationship between shear strength and scour volume exists, only samples with a water content between 26.7% and 27.3% were evaluated for Figs. 43 through 52. This minimized the variance in the study of the angle of inclination, distance from orifice and normal surface stress with respect to the volume of scour.

Comparing Figs. 43 through 45, it is seen that the volume of scour decreases with increasing separation distance between the orifice's discharge opening and the sample's surface. This inverse relationship is expected since the jet's kinetic energy will decrease with increasing distance from its source as predicted by Eq. 17. Thus, the tractive shear force will decrease with the weakening impinging jet, and the scour volume will decrease accordingly.

Furthermore, Figs. 43 through 45 show that for a given angle of inclination and distance from orifice, the volume of scour is approximately the same between the first two of three time durations,  $0 < V_o.t/d < 7.20 \times$

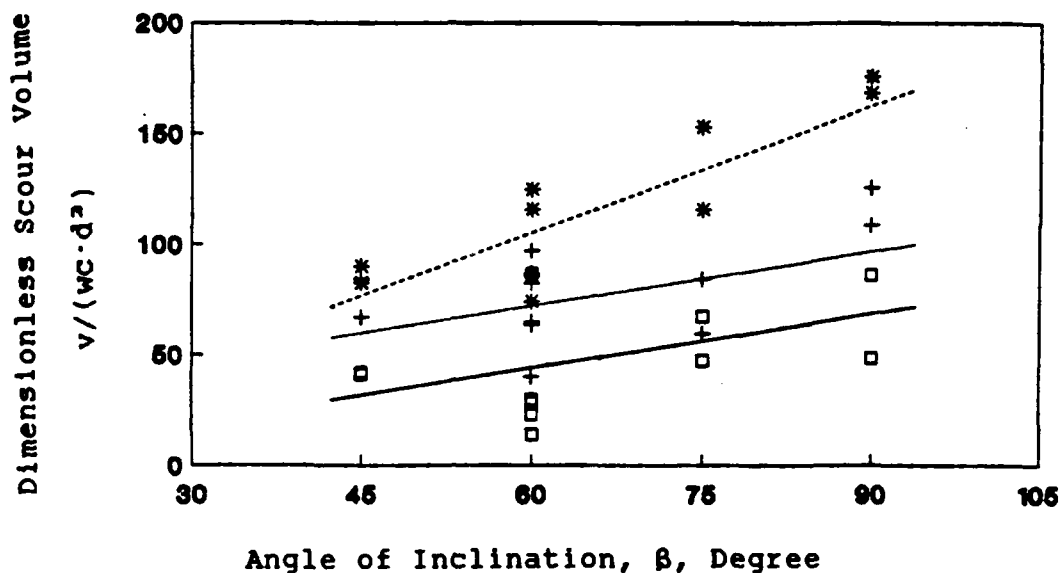


FIG. 43.-Dimensionless Scour Volume vs Angle of Inclination.  $z/d = 13.33$ .

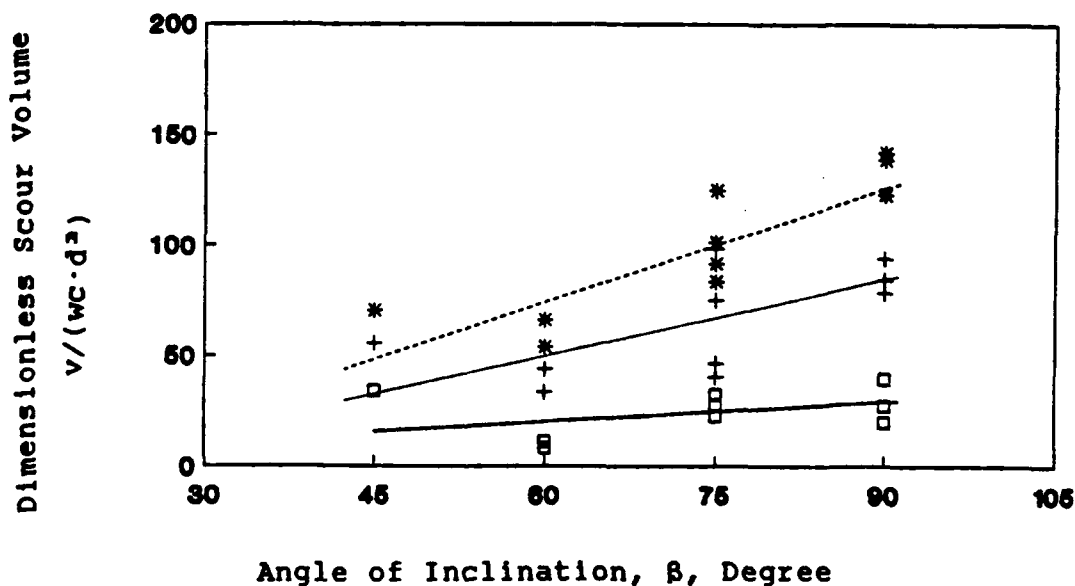


FIG. 44.-Dimensionless Scour Volume vs Angle of Inclination.  $z/d = 16.00$ .

26.7% < water content < 27.3%

- $V_o \cdot t/d = 7.20 \times 10^5$
- +—  $V_o \cdot t/d = 1.44 \times 10^6$
- \*—  $V_o \cdot t/d = 2.16 \times 10^6$

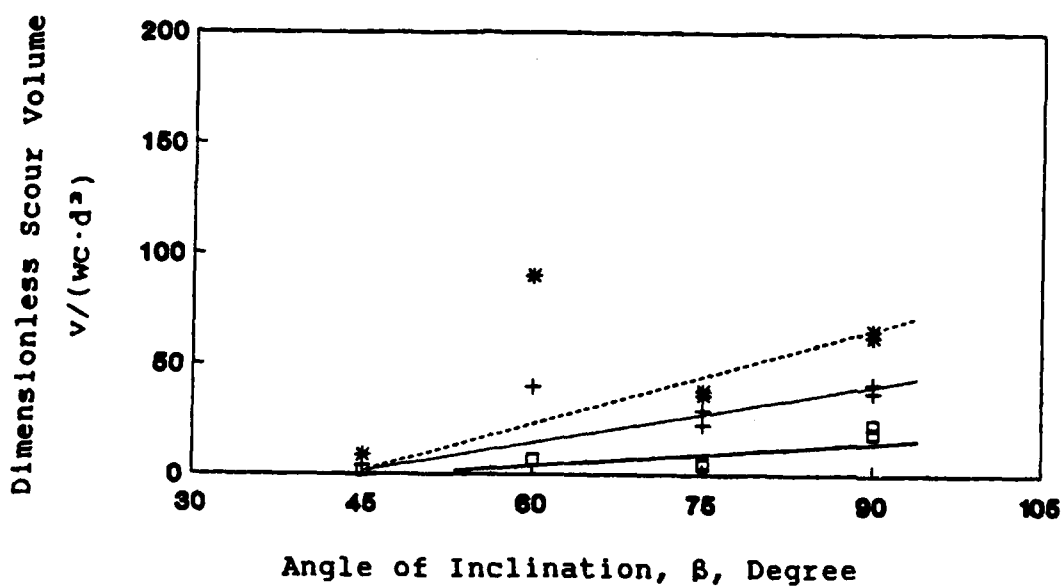


FIG. 45.-Dimensionless Scour Volume vs Angle of Inclination.  $z/d = 18.66$ .

26.7% < water content < 27.3%

- $V_o \cdot t/d = 7.20 \times 10^5$
- +—  $V_o \cdot t/d = 1.44 \times 10^6$
- \*—  $V_o \cdot t/d = 2.16 \times 10^6$

$10^5$ , and  $7.20 \times 10^5 < V_o.t/d < 1.44 \times 10^6$ . During the final time duration,  $1.44 \times 10^6 < V_o.t/d < 2.16 \times 10^6$ , the scour volume for large angles of inclination, is approximately equal to the scour volume of the prior two time durations. However, as the angle of inclination decreased, the scour volume for the final time duration also decreased. This would indicate that the scour cycle is transitioning to equilibrium conditions with decreasing angles of inclination. The transitional trend resulted from decreased tractive shear force with decreasing angle of inclination as shown by Fig. 24. As the scour cycle approached equilibrium, the volume of scour is expected to decrease. Also, the decreasing tractive shear force caused the total volume of scour to decrease with decreasing angle of inclination.

Figs. 46 through 48 verify the trends of Figs. 43 through 45, and show the scour volume is directly related to the tractive shear force.

In Figs. 43 through 48, the scour volume data for Sample Number B-I,  $\beta = 60^\circ$  and  $z/d = 18.66$ , is shown but not included in any linear regression or correlation. This sample's data is out of statistical control which might have resulted from an erroneous water content determination or inconsistent sample preparation.

#### SCOUR RATE

As stated in Chapter III, scour volume and rate are

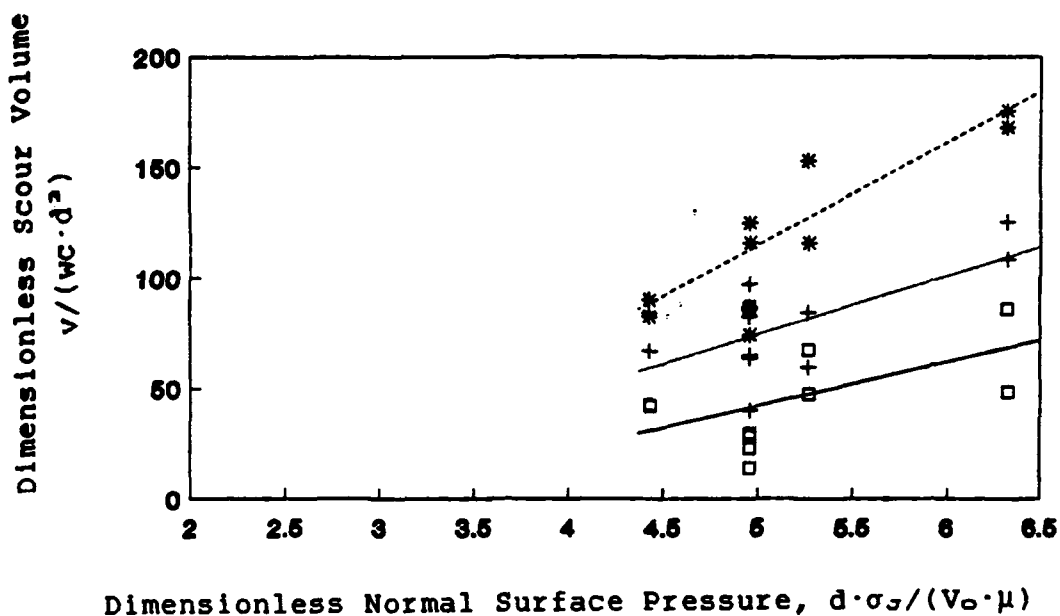


FIG. 46.-Dimensionless Scour Volume vs Normal Surface Pressure.  $z/d = 13.33$ .

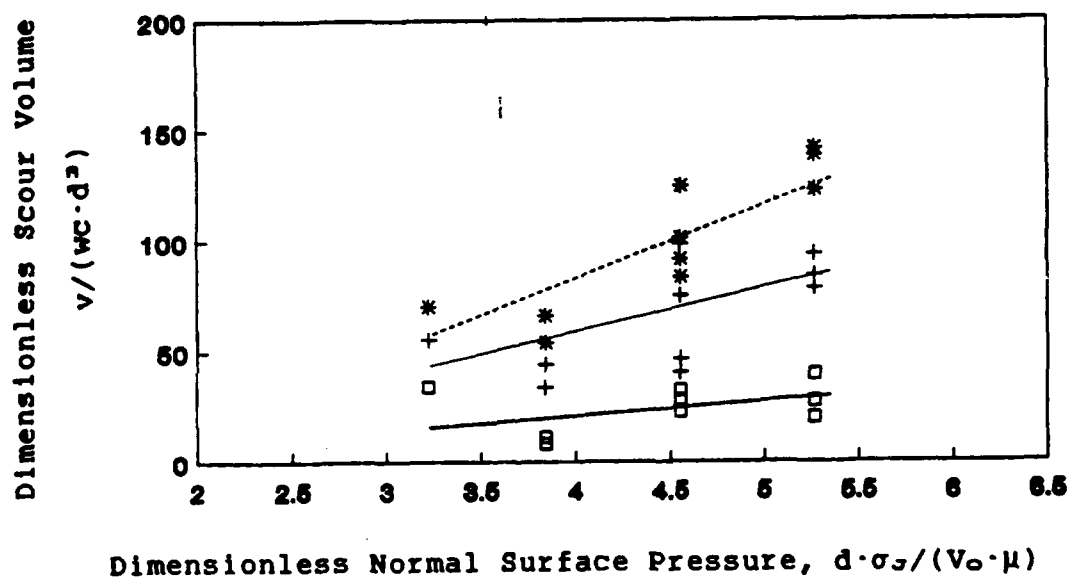


FIG. 47.-Dimensionless Scour Volume vs Normal Surface Pressure.  $z/d = 16.00$ .

26.7% < water content < 27.3%

- $\bullet$   $V_o \cdot t/d = 7.20 \times 10^5$
- $+$   $V_o \cdot t/d = 1.44 \times 10^6$
- $*$   $V_o \cdot t/d = 2.16 \times 10^6$

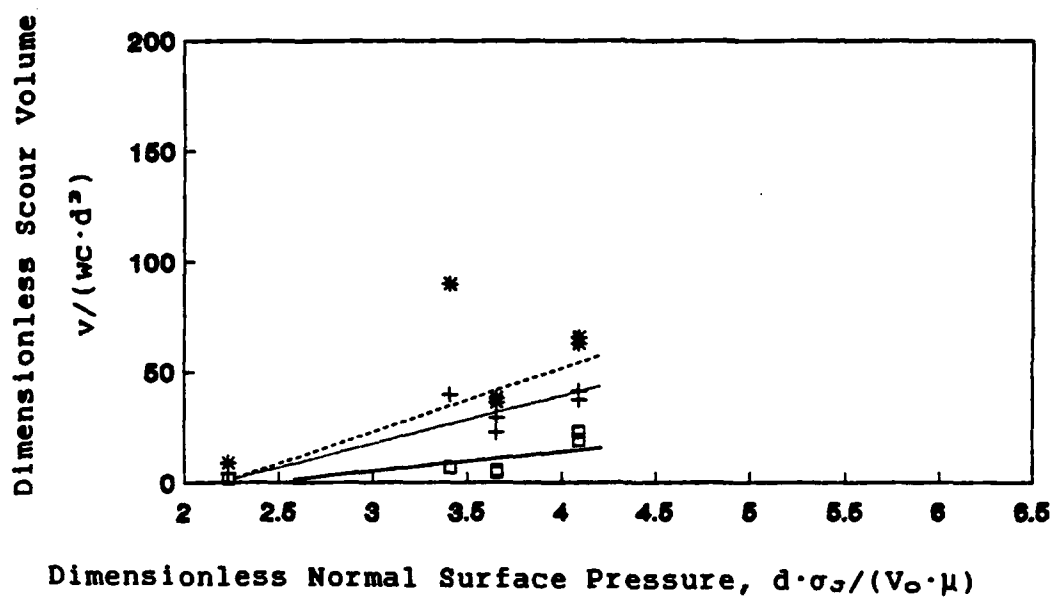


FIG. 48.-Dimensionless Scour Volume vs Normal Surface Pressure.  $z/d = 18.66$ .

26.7% < water content < 27.3%

- $V_0 \cdot t/d = 7.20 \times 10^5$
- +—  $V_0 \cdot t/d = 1.44 \times 10^5$
- \*—  $V_0 \cdot t/d = 2.16 \times 10^5$



functions of the same dimensionless pi terms, but the strength of their interdependencies varied as shown by Figs. 49 through 54. The rate of scour for each sample was calculated using the method of least squares to estimate the slope of linear relationship of scour volume to time of impingement. The origin was included in these calculations, since the samples with lower shear strengths had a high volume of scour during the first five minute duration when compared to the final five minute time durations. This is expected since the low shear strength sample would possess a lower critical tractive shear causing equilibrium conditions to be achieved quicker when compared to a sample with a higher shear strength.

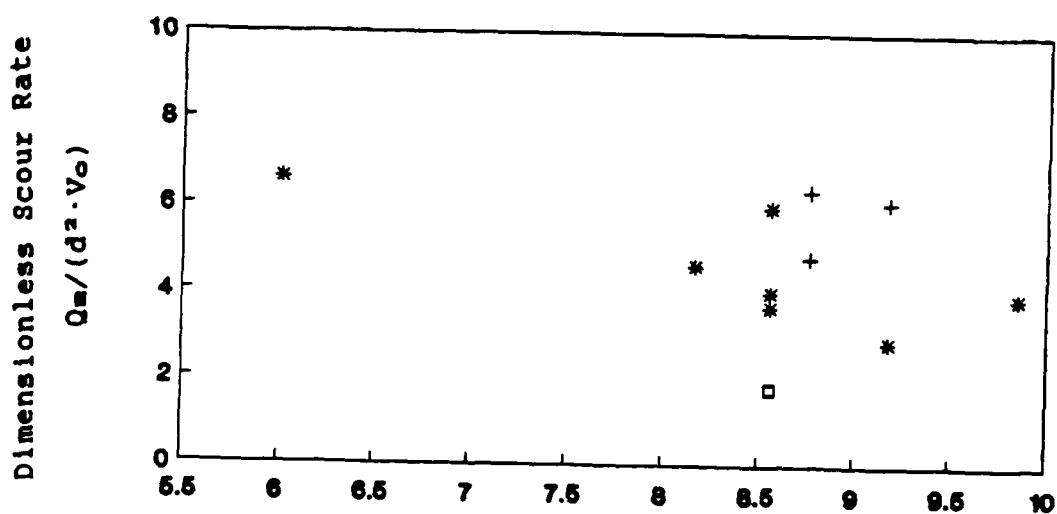
In general for a given angle of inclination, Figs. 49 through 52 show that no relationship existed between the sample's shear strength,  $\tau$ , and rate of scour,  $Q_s$ . However, if the data points for a given angle of inclination and separation distance are isolated, a relationship exist between scour rate and shear strength. The scour rate decreased with increasing shear strength, but a normal distribution of scour rates with respect to shear strengths existed. Furthermore, these isolated relationships are in agreement with Eq. 4 which predicts the scour rate as a function of shear strength.

Since a relationship between shear strength and scour rate exists, only samples with a water content between



Dimensionless Soil Shear Strength,  $d \cdot \tau / (V_o \cdot \mu)$

FIG. 49.-Dimensionless Rate of Scour vs Shear Strength.  
 $\beta = 90^\circ$ .



Dimensionless Soil Shear Strength,  $d \cdot \tau / (V_o \cdot \mu)$

FIG. 50.-Dimensionless Rate of Scour vs Shear Strength.  
 $\beta = 75^\circ$ .

- +  $z/d = 13.33$
- \*  $z/d = 16.00$
- $z/d = 18.66$
- x  $z/d = 21.33$

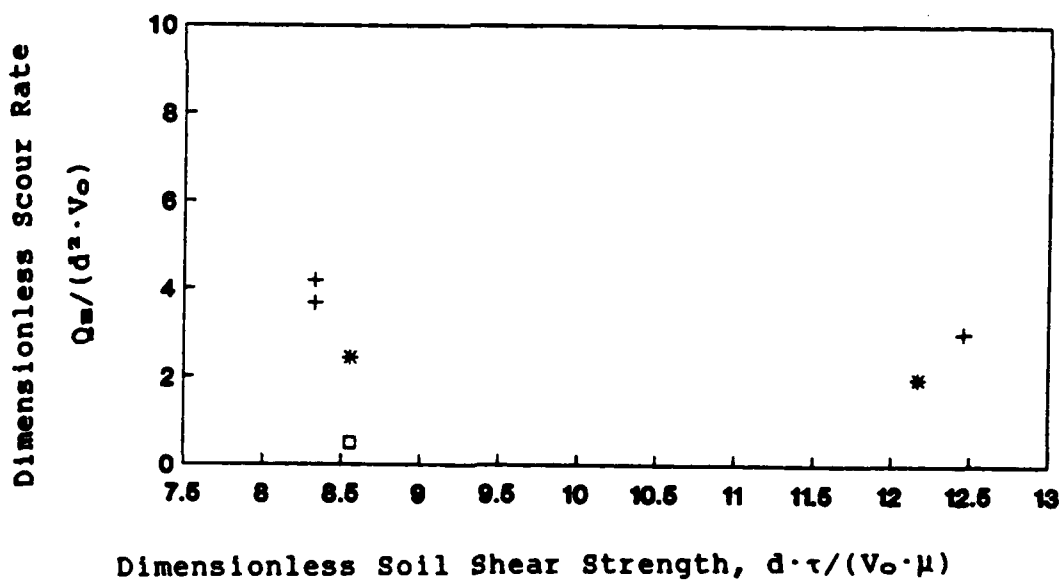
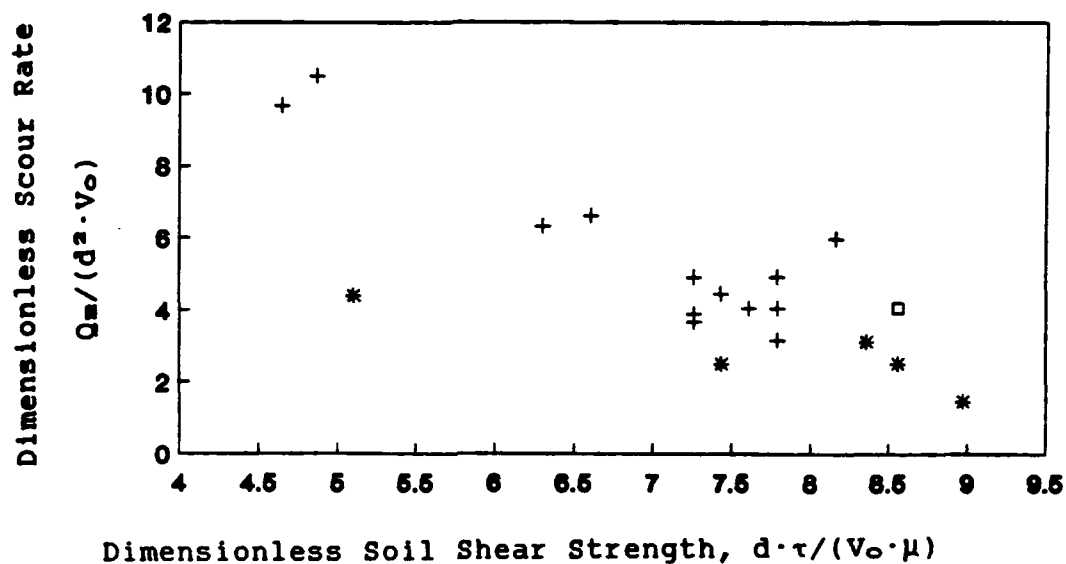


FIG. 52.-Dimensionless Rate of Scour vs Shear Strength.  
 $\beta = 45^\circ$ .

+  $z/d = 13.33$   
 \*  $z/d = 16.00$   
 □  $z/d = 18.66$

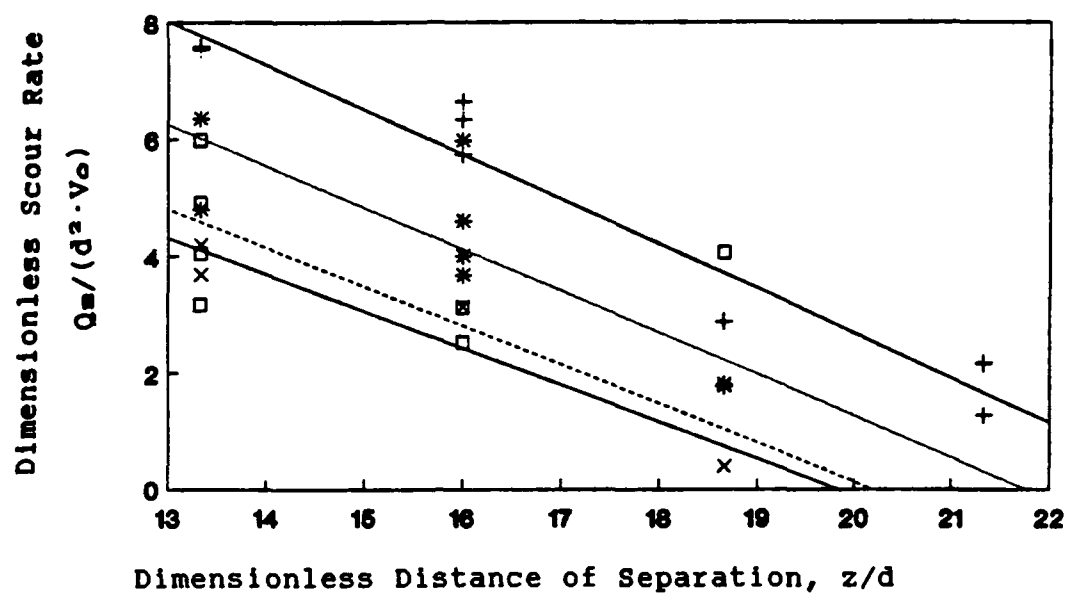


FIG. 53.-Dimensionless Rate of Scour vs Distance.

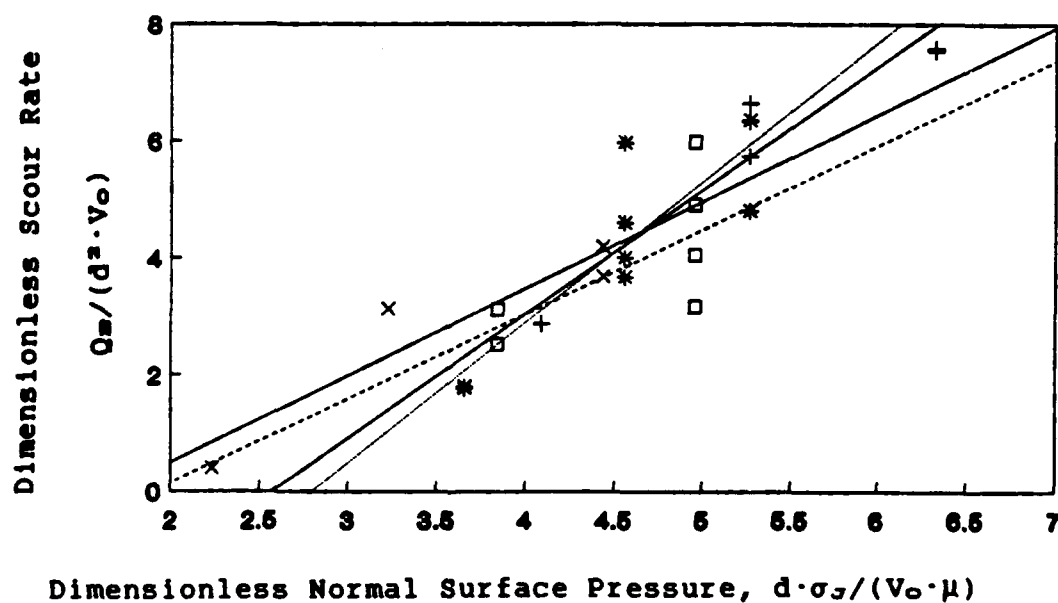


FIG. 54.-Dimensionless Rate of Scour vs Normal Surface Pressure.

26.7% < water content < 27.3%

- +  $\beta = 90^\circ$
- \*  $\beta = 75^\circ$
- $\beta = 60^\circ$
- x  $\beta = 45^\circ$

26.7% and 27.3% were evaluated for Figs. 53 through 54. This minimized the variance in the study of the angle of inclination, distance from orifice and normal surface stress with respect to the rate of scour.

Fig. 53 shows that the scour rate is a function of the angle of inclination and distance from the orifice's discharge opening to the sample. As the angle of inclination decreased and the distance from the orifice increased, the rate of scour decreased. This trend verifies Eq. 5 which predicts that the rate of scour will be a function of the initial jet velocity and distance to sample for a vertical jet.

As stated previously and shown by Fig. 24, reducing the angle of inclination and increasing the distance between orifice and jet, reduced the tractive shear force. Thus, the tractive shear force is the primary parameter governing the rate of scour. Fig. 54 verifies this statement. All four angles of inclination have approximately the same rate of scour for a given normal surface pressure. This indicates the rate of scour is dictated by the tractive shear force and not the angle of inclination.

Sample Number B-I,  $\beta = 60^\circ$  and  $z/d = 18.66$ , is shown in Figs. 49 through 54, but not included in any linear regression or correlation.

## SCOUR GEOMETRY

As predicted by Eq. 7 and shown by Figs. 55 through 60, the geometry of the scour hole was planer. The scour hole possessed large horizontal dimensions when compared to scour depth. In general, the scour hole was concentric about the center line of the jet for large angles of inclination, and became elliptical in shape for smaller angles of inclination. The majority of the scour volume was centered about the near-jet focal point for small angles of inclination.

The initial location of the scour hole for the majority of samples was slightly off the center line of the jet as indicated by Dunn (10). However, as the scour hole enlarged no precise repeating scour pattern boundaries could be predicted with respect to duration of impingement. In some cases this can be attributed to the joints in the multi-brick sample. The joints were the result of pressing four half bricks on the outer edges of a whole block. These joints inhibited scour of the half bricks and concentrated the scour to the center brick.

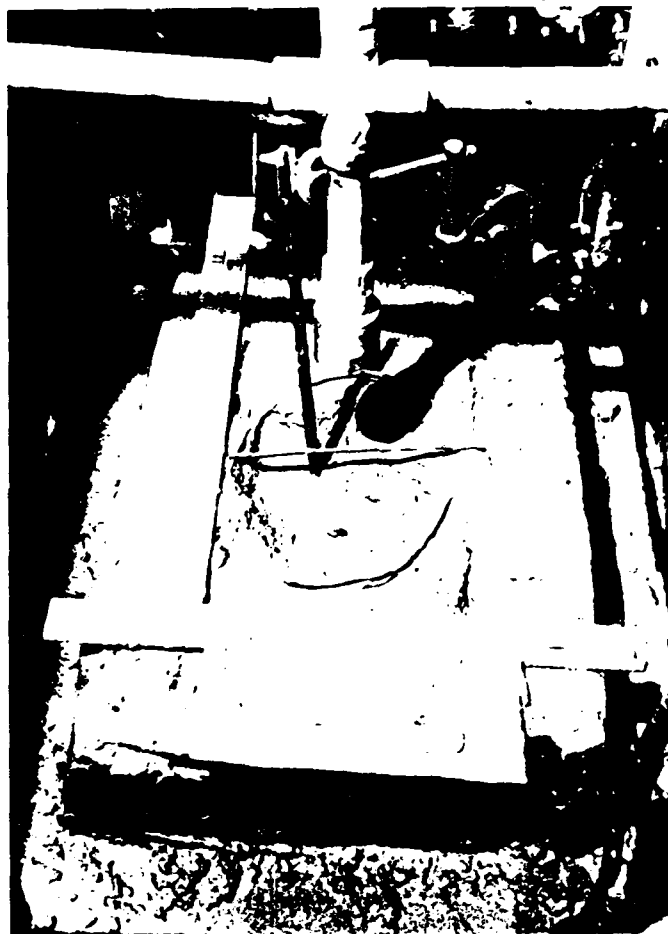


FIG. 55.-Scour. Sample No. B-III.

$$z/d = 16.00, \beta = 90^\circ, V_o \cdot t/d = 7.20 \times 10^5$$

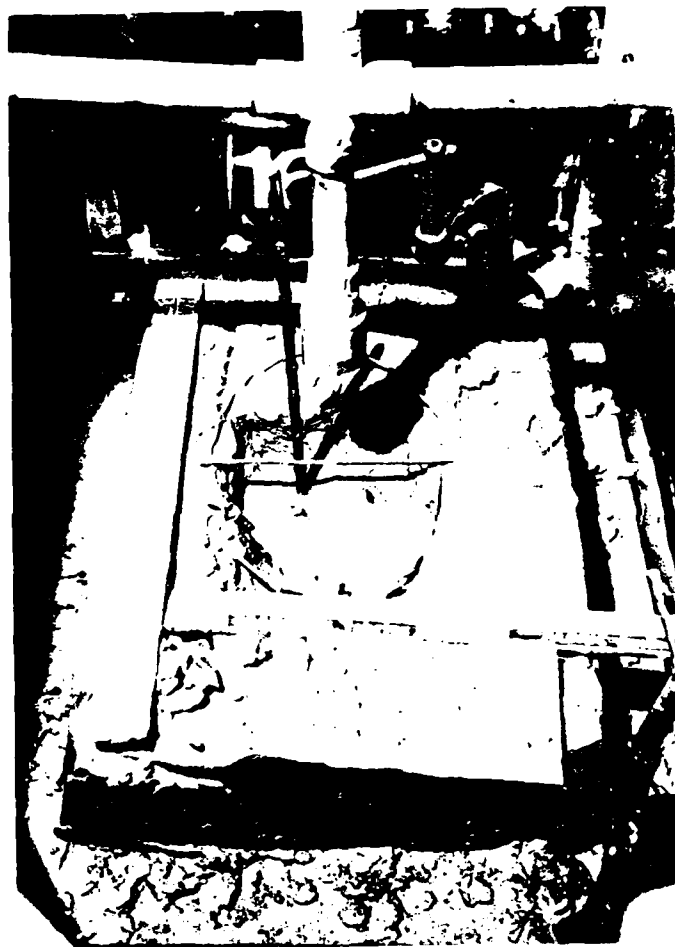


FIG. 56.-Scour. Sample No. B-III.  
 $z/d = 16.00$ ,  $\beta = 90^\circ$ ,  $V_o \cdot t/d = 1.44 \times 10^6$ .



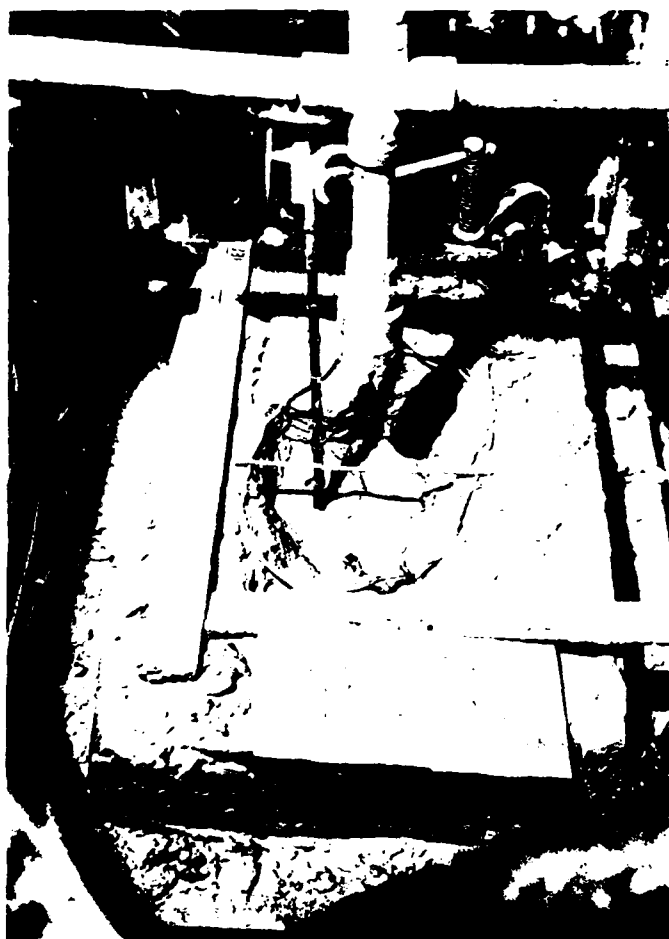


FIG. 57.-Scour. Sample No. B-III.  
 $z/d = 16.00$ ,  $\beta = 90^\circ$ ,  $V_o \cdot t/d = 2.16 \times 10^6$ .

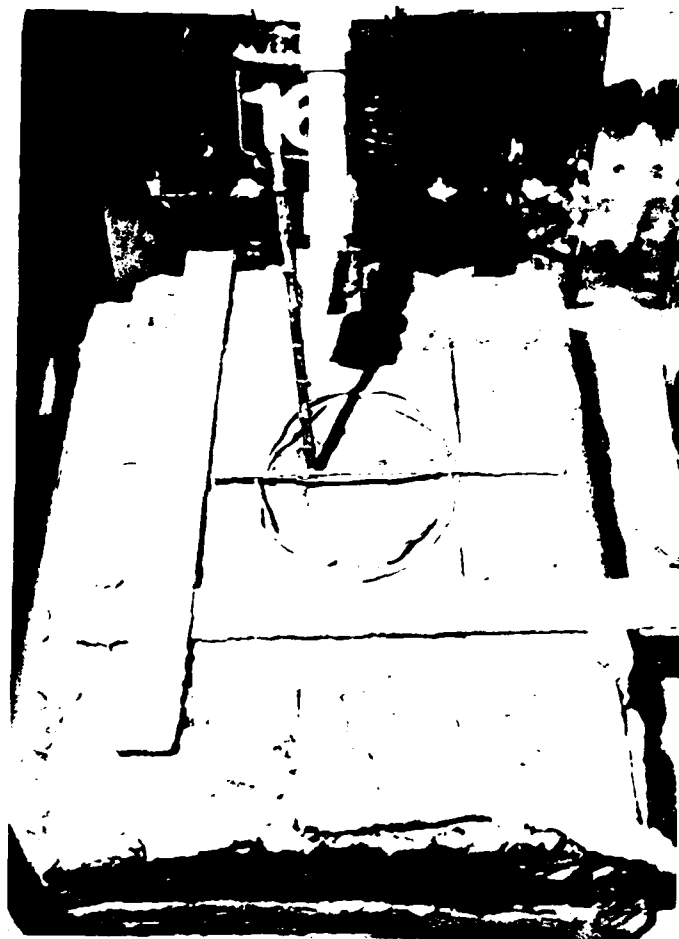


FIG. 58.-Scour. Sample No. B-I.  
 $z/d = 16.00$ ,  $\beta = 60^\circ$ ,  $V_o \cdot t/d = 7.20 \times 10^5$ .



FIG. 59.-Scour. Sample No. B-I.  
 $z/d = 16.00$ ,  $\beta = 60^\circ$ ,  $V_o \cdot t/d = 1.44 \times 10^6$ .



FIG. 60.-Scour. Sample No. B-I.

$$z/d = 16.00, \beta = 60^\circ, V_o \cdot t/d = 2.16 \times 10^6.$$

## CHAPTER VII

### CONCLUSIONS AND RECOMMENDATIONS

The specific objectives of this research were to study the governing parameters of incline scour of cohesive soils. The physico-chemical characteristics of clay, scour of cohesive soils, and mechanics of submerged turbulent radial jets were reviewed, followed by a descriptive presentation of incline scour of cohesive soils.

A model test consisting of three experiments was conducted. The first experiment was to determine the jet's velocity profile at various distances from the jet. These profiles were used to calculate the jet's initial velocity of 37.5 ft/sec. The profiles were similar to theory. The second experiment was to determine the normal surface pressure profiles resulting from the thrust of the impinging jet. The center line normal pressure was assumed to be representative of tractive shear force. The final experiment was to determine the primary governing parameters of incline scour. This was done by varying the time duration of scour impingement, shear strength of clay, distance of jet from sample, and angle of inclination of jet for Terra Cotta clay.

The model test resulted in the following conclusions:

- 1) Two mechanisms of scour apply to Terra Cotta clay. During the high tractive stress periods, the primary mechanism of scour was the detachment and removal of flat aggregate-like soil masses up to 1/4 inch thick. However, during the low tractive stress periods, the primary mechanism was particle by particle scour.
- 2) The volume of scoured material is linearly related to the time duration of impingement for the period of this experiment. This relationship is contrary to Masch and Moore (19), and Adbel-Rahmann's (1) findings. They stated a logarithmic relationship exists.
- 3) A relationship between the shear strength of clay and volume of scour was observed. A clay sample of high water content and low shear strength had a greater scour volume than a sample of low water content and high shear strength.
- 4) The volume of scour decreased for equal time durations as equilibrium conditions were approached.
- 5) The primary governing parameter of scour is tractive shear force caused by the impinging jet. Decreasing the angle of inclination and increasing the distance of separation between the orifice's discharge opening and the sample's surface decreased the volume of scour.

- 6) The rate of scour is primarily governed by the tractive shear force resulting from the jet's thrust. However, relationship did exist between the clay's shear strength and rate of scour.
- 7) The scour hole's geometry was concentric about the center line of the jet for large angles of inclination, and became elliptical in shape for smaller angles of inclination. The majority of the scour volume was centered about the near-jet focal point for small angles of inclination. However, in general as the scour hole enlarged no precise repeating scour pattern boundaries could be predicted with respect to duration of impingement.

The following are recommendations for further research:

- 1) Repeat the model test, but use a different scale to determine the scale effects associated with cohesive soils.
- 2) Repeat the model test using various clay types such as Na-montmorillonite and Ca-montmorillonite which possess varying mechanisms of scour. A comparison could then be made between the clays to determine if the scour volume and rate conclusions of this experiment apply to all clays. Also, the effects of varying Plastic Indexes with respect to scour volume and rate could be explored.

- 3) Repeat the model test using smaller angles of inclination.



## REFERENCES

1. Abdel-Rahmann, N. M., "The Effect of Flowing Water on Cohesive Beds," *Contribution No. 56*, Versuchsanstalt fur Wasserbau und Erdbau an der Eidgenossischen Technischen Hochschule, Zurich, Switzerland, 1964, pp. 1-114.
2. Abt, S. R., Ruff, J. F., and Shaikh, A., "Surface Erosion of Compacted Pure Clays," *Engineering Aspects of Soil Erosion, Dispersive Clays and Loess*, Geotechnical Special Publication No. 10, ASCE, New York, NY, 1984, pp. 67-78.
3. Albertson, M. L., Dai, Y. B., Jensen, R. A., and Rouse, H., "Diffusion of Submerged Jets," *Transactions Vol. 115*, ASCE, 1950, pp. 639-697.
4. Allen, T. L., and Keefer, R. M., *Chemistry: Experiment and Theory*, Harper and Row, Publishers, New York, NY, 1974, pp. 431-468.
5. Bhasin, R. N., Lovell, Jr., C. W., and Toebes, G. H., "Erodability of Sand-Clay Mixtures as Evaluated by a Water Jet," *Technical Report No. 8*, Purdue University, Water Resources Research Center, Lafayette, IN, 1969, pp. 3-59.
6. Bowels, J. B., *Engineering Properties of Soil and Their Measurements*, McGraw-Hill Book Company, New York, NY, 1978, pp. 15-27.
7. Cernica, J. N., *Geotechnical Engineering*, CBS College Publishing, New York, NY, 1982, pp. 20-26 and 238-304.
8. Denn, M. M., *Process Fluid Mechanics*, Prentice-Hall, Englewood Cliffs, NJ, 1980, pp. 112-114.
9. Dunlap, W. A., "Soil Mechanics in Dredging," *Dredging Engineering Short Course Lecture Notes*, Vol. I, Ocean Engineering Dept., Texas A&M University, College Station, TX, pp. DU-10 - DU-25.
10. Dunn, I. S., "Tractive Resistance of Cohesive Channels," *Journal of the Soil Mechanics Division*, ASCE, Jun., 1959, pp. 1-24.
11. Glauert, M. B., "Wall Jet," *Journal of Fluid Mechanics*, Vol. 1, 1956, pp. 625-643.

12. Herbich, J. B., *Coastal and Deep Ocean Dredging*, Gulf Publishing Company, Houston, TX, 1975, pp. 202-281.
13. Herbich, J. B., Private communication, 1990.
14. Holtz, R. D., and Kovacs, W. D., *An Introduction to Geotechnical Engineering*, Prentice-Hall, Englewood Cliffs, N.J., 1981, pp. 78-103 and 431-472.
15. Kobus, H., Leister, P., and Westrick, B., "Flow Field and Pulsating Jets Impinging on a Movable Bed," *International Association for Hydraulic Research*, Vol. 17, No. 3, pp. 175-193.
16. Langhaar, H. L., *Dimensional Analysis and Theory of Model Testing*, John Wiley and Sons, New York, NY, 1951, pp. 1-78.
17. Laursen, E. M., "Observations on the Nature of Scour," *Proceeding of the Fifth Hydraulics Conference*, ASCE, Jun., 1952, pp. 179-197.
18. Liou, Y., "Velocity Distribution and Movement Induced by Ship's Propeller in Ship Channels," *Proceedings of 25th Hydraulics Conference*, ASCE, Aug., 1977, pp. 228-236.
19. Masch, F. D., and Moore, W. L., "Experiments on the Scour Resistance of Cohesive Sediments," *Journal of Geophysical Research*, Vol. 67, No. 4, Apr., 1962, pp. 1437-1447.
20. Middleton, H. E., "Properties of Soils which Influence Soil Erosion," *USDA Technical Bulletin No. 178*, 1930, pp. 1-15.
21. Olsen, R. M., *Essentials of Engineering Fluid Mechanics*, Harper and Row, New York, NY, 1980, pp. 253-273 and 464-466.
22. Partheniades, E., "Erosion and Deposition of Cohesive Soils," *Journal of Hydraulics Division*, ASCE, Jan., 1965, pp. 105-139.
23. Pinson, J. L., "Bow Thruster Drives and Controls," *Naval Engineers Journal*, Vol. 75, No. 3, Aug., 1963, pp. 623-626.
24. Poreh, M., Tsuei, Y. G., and Cermak, J. E., "Investigation of a Turbulent Radial Wall Jet," *Journal of Applied Mechanics*, 1967, pp. 457-463.

25. Rajaratnam, N., *Turbulent Jets*, Elsevier Scientific Publishing Co., New York, NY, 1969, pp. 212-225.
26. Smerdon, E. T., and Beasley, R. P., "Critical Tractive Forces in Cohesive Soils," *Agricultural Engineering*, St. Joseph, MN, Jan., 1961, pp. 26-29.
27. Sowers, G. B., and Sowers, G. F., *Introductory Soil Mechanics and Foundations*, Macmillan Publishing Co., New York, NY, 1970, pp. 11-36 and 116-150.
28. Stuntz, G. R., and Taylor, R. J., "Some Aspects of Bow-Thruster Design," *Transactions Vol. 72*, The Society of Naval Architects and Marine Engineers, 1964, pp. 336-358.
29. Tausig, W. R., "Nearshore Trenching Technology Development", *Report TN No. N-1521*, Naval Construction Battalion Center, Port Hueneme, CA, Jun., 1978, pp. 20-27.
30. Taylor, D. W., *Fundamentals of Soil Mechanics*, John Wiley and Sons, New York, NY, 1960, pp. 362-479.
31. Vanoni, V. A., *Sedimentation Engineering*, ASCE, New York, NY, 1975, pp. 17-114.

**APPENDICES**

## APPENDIX I

## NOTATION

The following symbols are used in this thesis:

$A_o$	= Cross sectional area of orifice;	$[L^2]$
$A_1$	= cross sectional area at point 1;	$[L^2]$
$C_D$	= drained initial soil shear strength;	$[M/(L \cdot T^2)]$
$C_u$	= undrained initial soil shear strength;	$[M/(L \cdot T^2)]$
$C_1$	= scour constant;	
$C_2$	= scour constant;	
$d$	= diameter of jet nozzle or orifice;	$[L]$
$E_M$	= kinetic energy at a distance from the nozzle;	$[ML^2/T^2]$
$E_o$	= kinetic energy at nozzle;	$[ML^2/T^2]$
$g$	= gravity constant;	
$h$	= vertical distance of separation between sample and nozzle;	$[L]$
$h_L$	= pressure head lost;	$[L]$
$I_p$	= plastic index;	
$K$	= flow coefficient;	
$K_s$	= proportionality constant;	
$L$	= length;	$[L]$
$LL$	= liquid limit;	
$M$	= mass;	$[M]$
$P_o$	= pressure at orifice;	$[M/(L \cdot T^2)]$
$PL$	= plastic limit;	
$P_1$	= pressure at point 1;	$[M/(L \cdot T^2)]$
$Q$	= volumetric flow rate at nozzle;	$[L^3/T]$
$Q_m$	= volumetric erosion rate;	$[L^3/T]$
$Q_M$	= volumetric flow rate of entrainment at a distance from the nozzle;	$[L^3/T]$
$s$	= depth of scour depression;	$[L]$
$t$	= time duration of scour;	$[T]$
$T$	= time;	$[T]$
$v$	= volume of scour depression;	$[L^3]$
$V$	= velocity parallel to the jet axis at a radial distance from the center line;	$[L/T]$
$V_M$	= velocity parallel to the jet along the center line in the zone of established flow;	$[L/T]$
$V_o$	= velocity at nozzle or orifice;	$[L/T]$
$V_s$	= velocity parallel to the jet axis along the center line at a radial distance of one standard deviation;	$[L/T]$
$w_c$	= water content of soil;	
$x_j$	= horizontal distance from center line;	$[L]$
$y_j$	= horizontal distance from nozzle along center line;	$[L]$

$z$	= distance from nozzle to initial test sample surface;	[L]
$z_j$	= vertical distance from center line;	[L]
$\beta$	= angle of incline of jet from horizontal;	
$\pi$	= dimensionless parameter;	
$\sigma_s$	= standard deviation of velocity profile;	[L]
$\sigma_{T1}$	= triaxial of direct normal stress;	[M/(L·T <sup>2</sup> )]
$\sigma_{T2}$	= triaxial confining stress,	[M/(L·T <sup>2</sup> )]
$\sigma_j$	= normal center line stress on initial sample surface resulting from jet;	[M/(L·T <sup>2</sup> )]
$\rho$	= mass density of water;	[M/L <sup>3</sup> ]
$\tau$	= soil shear strength;	[M/(L·T <sup>2</sup> )]
$\tau_c$	= critical tractive shear;	[M/(L·T <sup>2</sup> )]
$\tau_T$	= triaxial or direct shear stress;	[M/(L·T <sup>2</sup> )]
$\tau_{TR}$	= tractive shear stress;	[M/(L·T <sup>2</sup> )]
$\mu$	= dynamic viscosity of water;	[M/(L·T)]
$\phi_D$	= drained angle of friction; and	
$\phi_U$	= undrained angle of friction.	

## APPENDIX II

## SCOUR ANALYSIS RESULTS

## SCOUR DATA

Angle of Inclination:  $\theta = 90^\circ$

z (inch)	2.5	2.5		
Sample Number	B-I	B-II		
Water Content (%)	26.8	26.7		
$\tau$ (lbs/ft <sup>2</sup> )	398	407		
t (min)	v (cubic inch)			
5	15.134	8.482		
10	22.152	19.100		
15	31.000	29.597		
$Q_m$ (ft <sup>3</sup> /sec)	0.0695	0.0690		

Angle of Inclination:  $\beta = 90^\circ$

z (inch)	3.0	3.0	3.0	
Sample Number	B-I	B-II	B-III	
Water Content (%)	27.1	27.1	27.1	
$\tau$ (lbs/ft <sup>2</sup> )	371	371	371	
t (min)	v (cubic inch)			
5	7.018	3.539	4.882	
10	16.782	15.073	14.035	
15	21.969	25.325	24.776	
$Q_m$ (ft <sup>3</sup> /sec)	0.0525	0.0608	0.0580	

z (inch)	3.5	3.5		
Sample Number	B-I	B-II		
Water Content (%)	27.1	27.2		
$\tau$ (lbs/ft <sup>2</sup> )	371	362		
t (min)	v (cubic inch)			
5	4.089	3.417		
10	6.713	7.445		
15	11.717	11.289		
$Q_m$ (ft <sup>3</sup> /sec)	0.0262	0.0263		



Angle of Inclination:  $\beta = 90^\circ$

z (inch)	4.0	4.0	4.0	
Sample Number	B-I	B-II	B-III	
Water Content (%)	27.0	27.1	27.2	
$\tau$ (lbs/ft <sup>2</sup> )	340	371	362	
t (min)	v (cubic inch)			
5	0.915	1.831	4.272	
10	2.136	5.492	7.262	
15	5.187	8.238	8.543	
$Q_m$ (ft <sup>3</sup> /sec)	0.0117	0.0197	0.0199	

Angle of Inclination:  $\theta = 75^\circ$

z (inch)	2.5	2.5	2.5	2.5
Sample Number	B-I	B-II	B-III	
Water Content (%)	26.5	26.7	26.7	
$\tau$ (lbs/ft <sup>2</sup> )	427	407	407	
t (min)	v (cubic inch)			
5	7.323	8.299	11.839	
10	18.307	10.496	14.829	
15	23.128	20.382	26.911	
$Q_m$ (ft <sup>3</sup> /sec)	0.0558	0.0440	0.0581	

z (inch)	3.0	3.0	3.0	3.0
Sample Number	B-I	B-II	B-III	B-IV
Water Content (%)	26.8	26.8	26.8	26.2
$\tau$ (lbs/ft <sup>2</sup> )	398	398	398	458
t (min)	v (cubic inch)			
5	4.821	4.882	3.967	3.722
10	17.392	7.140	8.238	10.496
15	22.030	15.378	16.171	14.890
$Q_m$ (ft <sup>3</sup> /sec)	0.0546	0.0336	0.0367	0.0357

Angle of Inclination:  $\theta = 75^\circ$

z (inch)	3.0	3.0	3.0	
Sample Number	C-I	E-I	G-I	
Water Content (%)	28.3	26.5	27.0	
$\tau$ (lbs/ft <sup>2</sup> )	280	427	380	
t (min)	v (cubic inch)			
5	12.510	2.746	5.736	
10	19.833	6.407	12.388	
15	26.606	11.411	18.002	
$Q_m$ (ft <sup>3</sup> /sec)	0.0605	0.0263	0.0421	

z (inch)	3.5	3.5		
Sample Number	B-I	B-II		
Water Content (%)	26.8	26.8		
$\tau$ (lbs/ft <sup>2</sup> )	398	398		
t (min)	v (cubic inch)			
5	0.915	0.793		
10	4.028	5.187		
15	6.713	6.407		
$Q_m$ (ft <sup>3</sup> /sec)	0.0161	0.0164		

Angle of Inclination:  $\theta = 60^\circ$

$z$ (inch)	2.5	2.5	2.5	2.5
Sample Number	A-I	A-II	B-I	B-II
Water Content (%)	27.5	27.3	27.0	27.2
$\tau$ (lbs/ft <sup>2</sup> )	337	354	380	362
$t$ (min)	$v$ (cubic inch)			
5	8.177	5.065	2.441	4.089
10	13.730	11.656	14.646	11.411
15	19.650	15.561	22.213	15.317
$Q_m$ (ft <sup>3</sup> /sec)	0.0448	0.0370	0.0548	0.0370

$z$ (inch)	2.5	2.5	2.5	2.5
Sample Number	C-I	C-II	D-I	D-II
Water Content (%)	27.9	28.1	27.2	27.5
$\tau$ (lbs/ft <sup>2</sup> )	307	293	362	337
$t$ (min)	$v$ (cubic inch)			
5	7.201	15.500	14.951	6.407
10	18.795	19.772	17.392	9.520
15	25.203	26.362	20.748	15.073
$Q_m$ (ft <sup>3</sup> /sec)	0.0606	0.0579	0.0449	0.0336

Angle of Inclination:  $\beta = 60^\circ$

$z$ (inch)	2.5	2.5	2.5	2.5
Sample Number	E-I	E-II	F-I	F-II
Water Content (%)	27.2	27.5	29.4	29.2
$\tau$ (lbs/ft <sup>2</sup> )	362	337	216	226
$t$ (min)	$v$ (cubic inch)			
5	5.309	5.553	33.197	27.949
10	7.201	8.970	39.543	34.539
15	13.242	15.927	40.398	43.937
$Q_m$ (ft <sup>3</sup> /sec)	0.0289	0.0356	0.0886	0.0961

$z$ (inch)	2.5			
Sample Number	G-I			
Water Content (%)	27.4			
$\tau$ (lbs/ft <sup>2</sup> )	345			
$t$ (min)	$v$ (cubic inch)			
5	8.482			
10	15.073			
15	16.904			
$Q_m$ (ft <sup>3</sup> /sec)	0.0398			

Angle of Inclination:  $\theta = 60^\circ$

$z$ (inch)	3.0	3.0	3.0	3.0
Sample Number	B-I	B-II	C-I	E-I
Water Content (%)	26.9	26.8	29.0	26.6
$\tau$ (lbs/ft <sup>2</sup> )	389	398	237	417
$t$ (min)	$v$ (cubic inch)			
5	1.953	1.465	5.065	1.159
10	7.811	5.980	9.337	2.990
15	11.717	9.520	17.880	5.797
$Q_m$ (ft <sup>3</sup> /sec)	0.0285	0.0230	0.0402	0.0133

$z$ (inch)	3.0			
Sample Number	G-I			
Water Content (%)	27.4			
$\tau$ (lbs/ft <sup>2</sup> )	345			
$t$ (min)	$v$ (cubic inch)			
5	5.797			
10	8.238			
15	10.130			
$Q_m$ (ft <sup>3</sup> /sec)	0.0228			

Angle of Inclination:  $\beta = 60^\circ$

z (inch)	3.5			
Sample Number	B-I			
Water Content (%)	26.8			
$\tau$ (lbs/ft <sup>2</sup> )	398			
t (min)	v (cubic inch)			
5	1.159			
10	7.018			
15	15.866			
$Q_m$ (ft <sup>3</sup> /sec)	0.0371			

Angle of Inclination:  $\theta = 45^\circ$

$z$ (inch)	2.5	2.5	2.5	
Sample Number	B-I	B-II	H-I	
Water Content (%)	26.9	26.9	25.2	
$\tau$ (lbs/ft <sup>2</sup> )	389	389	579	
$t$ (min)	$v$ (cubic inch)			
5	7.323	7.445	0.915	
10	11.900	14.890	5.309	
15	14.646	15.927	11.778	
$Q_m$ (ft <sup>3</sup> /sec)	0.0337	0.0384	0.0276	

$z$ (inch)	3.0	3.0		
Sample Number	B-I	H-I		
Water Content (%)	26.8	25.3		
$\tau$ (lbs/ft <sup>2</sup> )	398	566		
$t$ (min)	$v$ (cubic inch)			
5	6.041	1.343		
10	9.825	3.539		
15	12.449	6.530		
$Q_m$ (ft <sup>3</sup> /sec)	0.0286	0.0151		



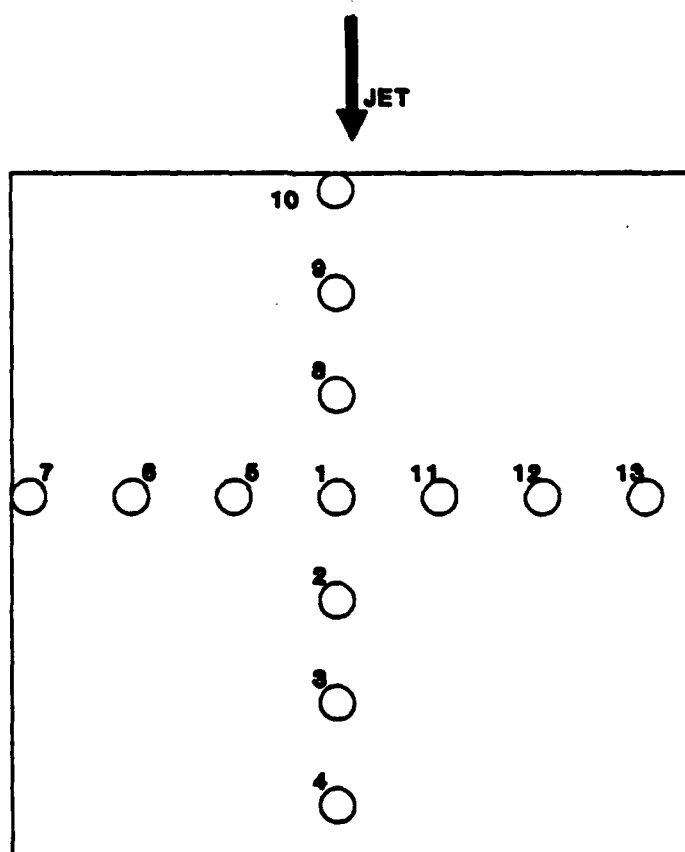
Angle of inclination:  $\theta = 45^\circ$

z (inch)	3.5			
Sample Number	B-I			
Water Content (%)	26.8			
$\tau$ (lbs/ft <sup>2</sup> )	398			
t (min)	v cubic inch)			
5	0.305			
10	0.732			
15	1.587			
Q <sub>av</sub> (ft <sup>3</sup> /sec)	0.0036			

## APPENDIX III

## THRUST ANALYSIS RESULTS

## THRUST DATA



Pressure Transducer Layout

Angle of Inclination:  $\beta = 90^\circ$

z (inch)	Pressure Transducer Number						
	1	2	3	4	5	6	7
	Normal Surface Stress, (psi)						
2.5	2.04	0.06	0.00	0.00	0.06	0.00	0.00
3.0	1.70	0.04	0.00	0.00	0.01	0.00	0.00
3.5	1.32	0.03	0.00	0.00	0.03	0.00	0.00
4.0	0.85	0.03	0.00	0.00	0.02	0.00	0.00

z (inch)	Pressure Transducer Number					
	8	9	10	11	12	13
	Normal Surface Stress, (psi)					
2.5	0.05	0.00	0.00	0.06	0.00	0.00
3.0	0.04	0.00	0.00	0.01	0.00	0.00
3.5	0.03	0.00	0.00	0.03	0.00	0.00
4.0	0.02	0.00	0.00	0.02	0.00	0.00

Angle of Inclination:  $\beta = 75^\circ$

z (inch)	Pressure Transducer Number						
	1	2	3	4	5	6	7
	Normal Surface Stress, (psi)						
2.5	1.70	0.02	0.00	0.00	0.03	0.00	0.00
3.0	1.47	0.02	0.00	0.00	0.02	0.00	0.00
3.5	1.18	0.02	0.00	0.00	0.01	0.02	0.00

z (inch)	Pressure Transducer Number					
	8	9	10	11	12	13
	Normal Surface Stress, (psi)					
2.5	0.00	0.00	0.00	0.02	0.00	0.00
3.0	0.00	0.00	0.00	0.02	0.00	0.00
3.5	0.01	0.00	0.00	0.01	0.00	0.00

Angle of Inclination:  $\theta = 60^\circ$

z (inch)	Pressure Transducer Number						
	1	2	3	4	5	6	7
	Normal Surface Stress, (psi)						
2.5	1.60	0.05	0.00	0.00	0.01	0.00	0.00
3.0	1.24	0.05	0.00	0.00	0.02	0.00	0.00
3.5	1.10	0.05	0.00	0.00	0.03	0.00	0.00

z (inch)	Pressure Transducer Number					
	8	9	10	11	12	13
	Normal Surface Stress, (psi)					
2.5	0.00	0.00	0.00	0.00	0.04	0.00
3.0	0.01	0.00	0.00	0.00	0.02	0.00
3.5	0.00	0.00	0.00	0.00	0.01	0.00

Angle of Inclination:  $\theta = 45^\circ$

z (inch)	Pressure Transducer Number						
	1	2	3	4	5	6	7
	Normal Surface Stress, (psi)						
2.5	1.43	0.06	0.00	0.00	0.00	0.03	0.00
3.0	1.04	0.05	0.00	0.00	0.00	0.18	0.00
3.5	0.72	0.02	0.00	0.00	0.00	0.23	0.00

z (inch)	Pressure Transducer Number					
	8	9	10	11	12	13
	Normal Surface Stress, (psi)					
2.5	0.03	0.00	0.00	0.01	0.00	0.00
3.0	0.00	0.00	0.00	0.01	0.00	0.00
3.5	0.00	0.00	0.00	0.00	0.00	0.00









Horizontal distance from nozzle:  $y_s = 0.5$  ft

Cross Sectional Distance

Vertical $z_s$ (ft)	Horizontal, $x_s$ , (ft)					
	right					
	0.10	0.15	0.20	0.25	0.30	0.40
Water Velocity, $V$ , (ft/sec)						
surface						
$C_L$ 0.00	1.67	0.66	0.67	0.56	0.58	0.64
bottom of tank						



Horizontal distance from nozzle:  $y_j = 1.0$  ft

Cross Sectional Distance

Vertical $z_j$ (ft)	Horizontal, $x_j$ , (ft)					
	right					
	0.10	0.15	0.20	0.25	0.30	0.40
Water Velocity, $V$ , (ft/sec)						
surface						
$C_L$ 0.00	3.17	2.88	1.05	0.82	0.76	0.73
bottom of tank						

## VITA

Name [REDACTED] : Joseph Delbert Hedges

[REDACTED]

[REDACTED]

Parents : Delbert Ross and Virginia Hedges

Education : B.S. Civil Engineering, 1983  
California State University, Chico

Profession : U.S. Naval Officer, Civil Engineer  
Corps

[REDACTED]